

A Radio Assay for the Study of Radio Frequency Tag Antenna Performance

A Thesis
Presented to
The Academic Faculty

by

Joshua David Griffin

In Partial Fulfillment
of the Requirements for the Degree
Master of Science in Electrical and Computer Engineering

School of Electrical and Computer Engineering
Georgia Institute of Technology
August 2005

A Radio Assay for the Study of Radio Frequency Tag Antenna Performance

Approved by:

Dr. Gregory D. Durgin, Adviser
School of Electrical and Computer Engineering
Georgia Institute of Technology

Dr. Andrew F. Peterson
School of Electrical and Computer Engineering
Georgia Institute of Technology

Dr. Emmanouil M. Tentzeris
School of Electrical and Computer Engineering
Georgia Institute of Technology

Date Approved: May 2005

*To David and Ellen Griffin,
for their encouragement and support.*

ACKNOWLEDGEMENTS

This report would not have been possible without the advice, assistance, and encouragement from others. I would like to thank my advisor, Greg Durgin, for his guidance and encouragement and Professor Bernard Kippelen for his role in conceptualizing the project. In addition, I owe a great debt to Andreas Haldi for building many revisions of the RF tag antennas. I would also like to recognize Yenpao “Albert” Lu for his excellent horn antennas and his assistance in taking measurements and Joel Prothro for his hard work on material measurements. I also thank Professor Kenney, Minsik Ahn, and Pasha for providing equipment for the experiments and Bob House for machining several circuits and antennas.

TABLE OF CONTENTS

ACKNOWLEDGEMENTS	iv
LIST OF TABLES	vii
LIST OF FIGURES	viii
SUMMARY	xi
I THE RADIO FREQUENCY TAG SYSTEM	1
1.1 Introduction	1
1.2 The RF Tag System	1
1.2.1 Reader	2
1.2.2 RF Tags	2
1.2.3 Tag Operating Frequencies	7
II CURRENT RF TAG CHALLENGES AND RESEARCH	9
2.1 Tag Cost	9
2.2 Tag Footprint	10
2.3 Tag Performance	10
III THE RADIO ASSAY	13
3.1 The Radio Assay Defined	13
3.2 General Equipment for the Radio Assay	14
3.2.1 RF Tag Antenna	14
3.2.2 Balun and Transmission Line Topology Transformer	19
3.2.3 Tunable Impedance Transformation Network	27
3.2.4 Directional Antennas	40
3.2.5 Antenna Range	41
IV EXPERIMENTAL METHODS	43
4.1 Radio Assay Equipment Setup	43
4.2 RF Tag Antenna Feed and Attachment	44
4.3 Antenna Range Modifications	45
4.4 Radio Assay Materials	48
4.5 Radio Assay Calibration	51
4.6 Calculations	54

4.7	RF Tag Antenna Orientation	57
V	RESULTS AND DISCUSSION	59
5.1	RF Tag Antenna Performance versus Antenna Material and Manufacturing Methods	59
5.2	RF Tag Antenna Performance versus Material Attachment	61
5.3	Antenna Performance versus Impedance Tuning	63
5.4	Guidelines for RF Tag Design	64
VI	CONCLUSION AND SUGGESTED FUTURE WORK	70
6.1	Conclusion	70
6.2	Suggested Future Work	70
	APPENDIX A — TABULATED DATA FROM THE RF TAG ANTENNA MATERIAL MEASUREMENTS	72
	REFERENCES	83

LIST OF TABLES

1	ISM band frequencies available for RF tag system use	8
2	Physical causes of RF tag antenna performance degradation	11
3	RF tag antenna physical characteristics	19
4	Pertinent S parameters of quarter wave balun and balance test board for balun performance characterization	26
5	S parameters of two back-to-back quarter wave baluns	27
6	Complex permittivity of materials for radio assay experiments	49
7	RF tag antenna performance characteristics in free space	59
8	RF tag antenna physical characteristics reprinted from Table 3	61
9	Range of the decrease in the front region linearly averaged RF tag antenna gain due to material losses	62
10	Range of the decrease in the linearly averaged RF tag antenna gain when the tunable impedance transformation network was tuned to the material and when it was tuned to freespace	64
11	Return loss and percentage of power lost due to the impedance mismatch of free space tuned antennas when attached to various materials	66
12	RF tag antenna performance characteristics when attached to 1.5 inch thick cardboard	73
13	RF tag antenna performance characteristics when attached to 1.32 inch thick acrylic	73
14	RF tag antenna performance characteristics when attached to 1.32 inch thick wood	77
15	RF tag antenna performance characteristics when attached to a cardboard carton filled with water	77
16	RF tag antenna performance characteristics when attached to beef enclosed in a plastic bag	80
17	RF tag antenna performance characteristics when attached to cardboard carton filled with ethylene glycol	80
18	RF tag antenna performance characteristics when attached to metal	82

LIST OF FIGURES

1	(a) One-bit and (b) multiple-bit RF tag operating mechanisms	4
2	Field regions of a radiating element	6
3	(a) Near field inductive coupling RF tag system communication and (b) far-field backscatter RF tag system communication	7
4	Passive RF tag performance metrics	11
5	Cross section of coplanar strip (CPS) transmission line	15
6	Folded dipole decomposed into the (a) transmission line mode and (b) antenna mode for impedance analysis	16
7	Printed folded dipole dimensions for 915MHz	17
8	915 MHz electroless silver flexible folded dipole in acetone bath to remove printed mask	18
9	Flexible 915 MHz folded dipole made from electroless silver deposited on a PET substrate	19
10	Transparent and flexible 915 MHz folded dipole antenna made from indium tin oxide (ITO) deposited on a PET substrate	20
11	Flexible electroless copper 915 MHz folded dipole deposited on a PET substrate	20
12	Rigid baseline 915 MHz folded dipole milled on copper-clad FR4 substrate	21
13	Balanced and unbalanced systems and their connection	22
14	Quarter wave balun with folded dipole connected to the balanced terminals . . .	23
15	Quarter wave balun equivalent circuits	24
16	Equivalent circuit and currents on the balun amplitude and phase test board . .	25
17	Quarter Wave Balun and Balance Test Board	26
18	Balun ratio of quarter wave balun versus frequency	27
19	Diagram of back-to-back quarter wave balun measurement that shows how S21 and S12 of the back-to-back measurement were attributed equally to each balun	28
20	Arbitrary transmission line with load Z_{load} driven by a voltage source V_{gen} with an internal impedance Z_{gen}	28
21	Equivalent circuit of an arbitrary transmission line with input impedance Z_{in} driven by a voltage source V_{gen} with an internal impedance Z_{gen}	30
22	Equivalent circuit of two cascaded, arbitrary transmission lines of characteristic impedance Z_a and Z_b	31
23	Equivalent circuit of transmissions line shown in Figure 22 with Z_b and Z_{load} reduced to Z_{in-b}	31

24	Equivalent circuit of transmissions line shown in Figure 23 with Z_{in-b} and Z_a reduced to Z_{in_a}	32
25	Diagram of general impedance matching network	32
26	General lossless impedance and admittance matching network equivalent circuits	33
27	General tunable Pi impedance transformation circuit	34
28	Tunable impedance transformation circuit using varactor diodes for capacitors and two J inverters to transform the center capacitance into an inductance . . .	35
29	J inverter equivalent circuit	35
30	(a) Varactor diode bias network and (b)impedance transformation board layout .	36
31	(a) Tunable impedance transformation network board and (b) tunable impedance transformation network box with directional couplers at the input and output . .	37
32	Tunable impedance transformation network control box (a) schematic and (b) photo	38
33	Tunable impedance transmission network with return loss and insertion loss direction couplers for feedback	39
34	915 MHz horn antenna with 40°beamwidth and 10.1 dBi peak gain.	40
35	Outdoor antenna range diagrams	42
36	Diagram of radio assay experimental setup	44
37	Quarter wave balun balanced terminals connected to the CPS transmission line antenna feed for the RF tag antennas	46
38	RF tag antenna attached to solid material	46
39	RF tag antenna attached to the liquid container	47
40	Side view of outdoor antenna range	48
41	Interpolated (a) permittivity and (b) loss tangent values from Von Hippel	50
42	Electroless silver antenna attached to wood which is attached to the RF tag antenna mount	52
43	Baseline antenna on beef attached to the RF tag antenna mount	52
44	Electroless silver antenna attached to a milk carton on the RF tag antenna mount	53
45	Equipment connections for the back-to-back calibration of the radio assay experimental setup	55
46	RF tag antenna E and H plane cuts	57
47	RF tag antenna orientation when attached to a material	58
48	Far field pattern of RF tag antenna patterns in free space	60
49	Method for calculating the average RF tag antenna gain penalty due to material loss	62
50	Free space and material tuned RF tag antenna gain penalties	65

51 Return loss of free space tuned antennas when attached to various materials . . . 67

52 Diagram of an RF tag system far field backscatter communication link between
a reader's transmit and receive antennas and an RF tag 68

53 Four RF tag antennas attached to 1.5 inch thick Cardboard 72

54 Four RF tag antennas attached to 1.32 inch thick acrylic 74

55 Four RF tag antennas attached to 1.32 inch thick wood 75

56 Four RF tag antennas attached to cardboard carton filled with water 76

57 Four RF tag antennas attached to beef enclosed in a plastic bag 78

58 Four RF tag antennas attached to a cardboard carton filled with ethylene glycol 79

59 Three RF tag antennas attached to metal 81

SUMMARY

In recent years, passive radio frequency (RF) tags that communicate using modulated backscatter radiation have shown great potential for use in inventory management, parcel and postal tracking, for use as remote sensors, and in a host of other Radio Frequency Identification (RFID) applications. However, for the widespread use of these tags to become reality, much basic research is needed to reduce the cost, increase the range, and increase the reliability of the RF tag. This research seeks to enhance the performance of passive RF tags by developing a series of tests, or radio assay, to measure the following: the performance of RF tag antennas as a function of antenna material and manufacturing technique and the antenna performance when attached to various materials. The radio assay experiments are designed for RF tag antennas that operate in the far field of the tag reader and communicate using modulated backscatter radiation at 915 MHz. Three flexible, folded dipoles, printed on plastic substrates, were measured in the radio assay experiments. The results of the experiments include the following: the antenna gain penalty (relative to a baseline antenna) for each antenna material and manufacturing technique, the antenna gain penalty (relative to the free space antenna gain) due to material losses when the tag antenna is attached to an object, and the benefits (in terms of antenna gain) of tuning each tag antenna to the material to which it is attached. The results are presented in a form to aid RF engineers in the design of RF tag system link budgets.

CHAPTER I

THE RADIO FREQUENCY TAG SYSTEM

1.1 Introduction

Radio Frequency (RF) tags are transponders that communicate with an interrogator, or reader, using electric fields, magnetic fields, or far field electromagnetic radiation [1]. RF tags find their use in two broad applications: sensors and radio frequency identification (RFID). In recent years, RFID applications of RF tags have generated increasing interest because of their potential applications to inventory management, parcel and postal tracking, non-stop toll collection, access control, document identification, airport luggage, self check out, theme parks, library items, and medical ID bracelets [2, 3, 4]. Their use is expected to increase dramatically in the coming years due to mandates by Wal-Mart and the Department of Defense for their suppliers to begin using RFID tags on their shipments [5, 6]. Although these entities desire to label and track individual items in their inventory, the relative high cost and poor performance of RF tags limit their use to tracking at the pallet or crate level [7, 8]. For item level tracking to become reality, much research is needed to lower the tag cost, reduce the tag footprint, and improve the tag performance and reliability. One of the most important factors that affects the overall RF tag performance is the performance of the RF tag antenna. The antenna performance is reduced by antenna deformation, polarization mismatch, and the electromagnetic properties of the tagged object. This report presents a series of tests, or radio assay, to measure the performance of RF tag antennas as a function of antenna material and manufacturing method and the antenna performance when attached to various materials.

1.2 The RF Tag System

RF tag systems vary widely in their use and design, making it difficult to compile an exhaustive overview of the subject. However, a basic knowledge of these systems is necessary to understand and appreciate the work presented in this report. To this end, it is worth mentioning that much of the media coverage of RFID tags presents them as a new type of technology. However, RFID

tags are simply one application of general RF tags which have existed for several years. Although the principles discussed in this report apply to general RF tags, the material will be presented with RFID applications in mind. The remainder of this chapter provides a brief overview of the types and common components of basic RF tag systems.

1.2.1 Reader

All RF tag systems consist of a reader and a tag. The reader is used to communicate with the tag and make tag information available in a digital format. This information may be a code stored on the tag or, as in the case of a 1-bit tag, simply that the tag is present in the reader's read zone [3]. All readers consist of the following components:

- Hardware and software to make tag data available in a digital format
- Hardware and software to control communication with the tag
- Antenna(s) to enable wireless communication with the tag

Depending upon the type of RF tag, the reader may also be used to program, enable or disable, and supply power to the tag.

1.2.2 RF Tags

1.2.2.1 1-Bit Tags

The RF tag is a transponder whose function is to communicate its information to the reader when interrogated by a radio signal. Many different types of RF tags are available for RFID applications. The most basic tags are 1-bit tags that simply alert the reader to the tag's presence in the reader's read zone, shown in Figure 1a. These passive tags are often used in electronic article surveillance (EAS) applications and usually do not contain an integrated circuit [1]. One-bit tags are detected in the reader's read zone by exploiting properties of resonant circuits or the physical properties of a material [1, 4]. For example, tags that operate in the near field of the reader via inductive coupling (Section 1.2.2.2), sweep the frequency of the field in order to detect a tag containing a resonant circuit or a material that exhibits non-linearities. When the frequency is swept past a resonance or non-linearity, the reader detects an abrupt change in its reader coil impedance. In addition, some tags may use a basic frequency division chip to generate a frequency at some multiple of the carrier frequency. Tags that operate in the far

field of the reader (Section 1.2.2.2) use non-linear devices such as diodes to generate harmonics that are detected by the reader.

1.2.2.2 Multiple-Bit Tags

All other tags are capable of transmitting a multiple-bit code to the reader. These tags usually consist of power supply circuitry, a memory storage device, an antenna, and modulation circuitry, shown in Figure 1b.

Power Supply RF tags can be classified as active or passive depending upon the type of power supply used [9]. Active tags use an on-board power source (battery or solar cell) to operate the circuitry that stores and modulates the information in the tag. Active tags should not be confused with RF beacons, which use their power supply to operate an active RF stage to retransmit a radio signal. Such beacons are not considered RF tags and are outside the scope of this report. In contrast to active tags, the only source of power for passive tags is the field or far field radiation provided by the tag reader. Active tags have the advantage of increased read range when compared to passive tags. However, passive tags are much less expensive than active tags and can operate indefinitely [9].

Most tag power supplies use a rectifying stage to convert the received wave into a DC voltage to power the onboard circuitry. Since the received power is usually very small, an efficient rectification stage is required. However, some tags avoid the rectification stage altogether by powering the tag circuitry directly from the AC voltage generated at the antenna terminals of the tag [10, 11]. In addition, tags that use surface acoustic wave (SAW) techniques to create a coded signal are completely passive, do not contain an integrated circuit, and therefore do not require a power supply [4].

Memory Storage The memory storage of an RF tag is used to store the multiple-bit identification code that is to be communicated to the reader. Tags that cannot be reprogrammed use state machines or read only memories (ROM) to store or generate the information. Rewritable, inductively coupled RF tags commonly use electrically erasable and programmable read-only memory (EEPROM) while active, backscatter tags typically use SRAM to store digital codes [1].

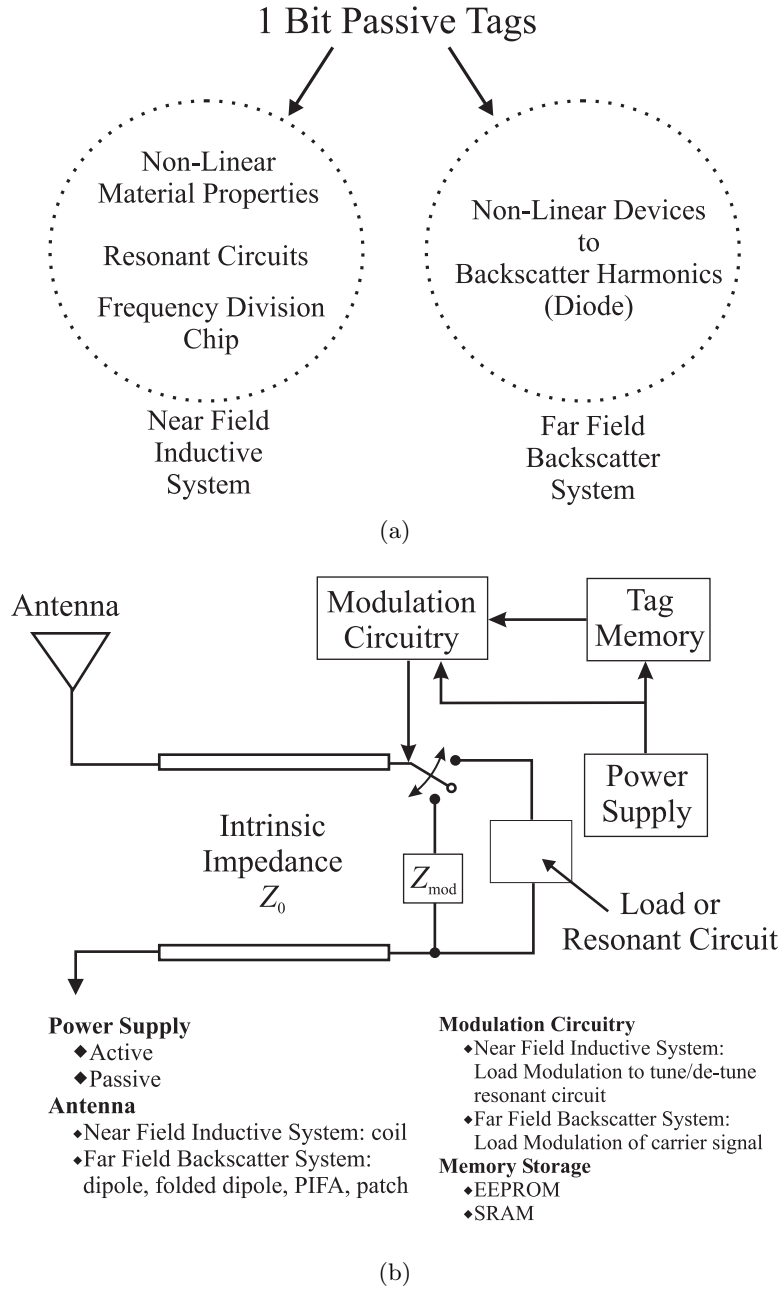


Figure 1: (a) One-bit and (b) multiple-bit RF tag operating mechanisms

Antenna The type of antenna used in the RF tag depends upon the field or radiation that is being employed for tag communication. The general expression for the fields radiating from a current filament can be described as follows [12]:

$$\tilde{\mathbf{H}} = \frac{I\Delta z}{4\pi} \left[\frac{j\beta}{r} + \frac{1}{r^2} \right] e^{-j\beta r} \sin(\theta) \hat{\phi} \quad (1)$$

$$\begin{aligned} \tilde{\mathbf{E}} &= \frac{I\Delta z}{4\pi} \left[\frac{j\omega\mu}{r} + \sqrt{\frac{\mu}{\epsilon}} \frac{1}{r^2} + \frac{1}{j\omega\epsilon r^3} \right] e^{-j\beta r} \sin(\theta) \hat{\theta} \\ &+ \frac{I\Delta z}{2\pi} \left[\sqrt{\frac{\mu}{\epsilon}} \frac{1}{r^2} + \frac{1}{j\omega\epsilon r^3} \right] e^{-j\beta r} \cos(\theta) \hat{\mathbf{r}} \end{aligned} \quad (2)$$

where

I = the constant amplitude of the current filament oriented in the positive z direction

Δz = the length of the current filament

β = phase constant, $2\pi/\lambda$, where λ is the wave-length

r = the radial distance from the current filament

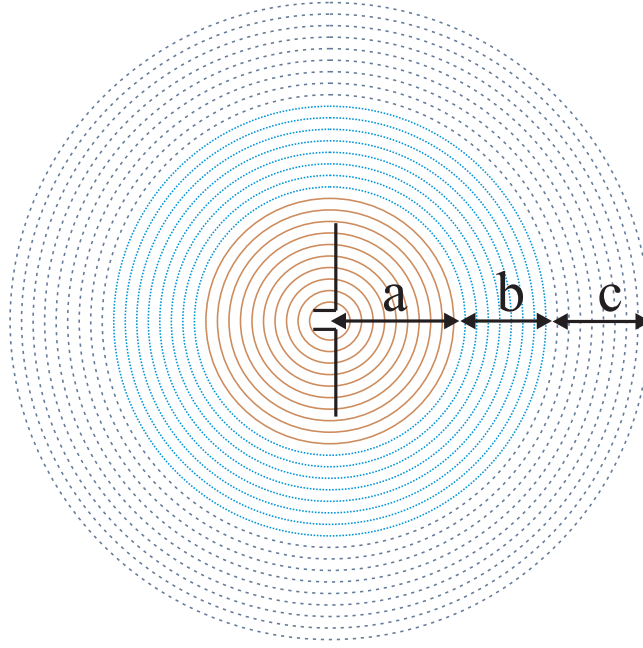
ω = radian frequency

μ = permeability of the medium

ϵ = the permittivity of the medium

Reactive near fields, Figure 2, are standing waves that do not radiate power, but store energy in the volume very near to the antenna. In (1) and (2), the reactive near fields are represented by those terms that decay as $1/r^3$. Typically, the reactive near field region is taken to be $0.62\sqrt{D^3/\lambda}$ where D is the largest dimension of the antenna and $D \gg \lambda$ [12]. Just outside of the volume containing the reactive near field is the Fresnel region. This region contains both standing wave and traveling waves. These fields decay as $1/r^2$ and typically extend to $2D^2/\lambda$ [12]. The region that extends from the end of the Fresnel region to $r = \infty$ is the Fraunhofer or far field region [12]. These radiating far-fields are traveling waves that carry power away from the antenna. These fields decay at a rate of $1/r$.

For a tag to operate in the reactive near field, the tag antenna consists of several loops of wire, or a coil which allows the tag to be powered by inductive coupling. In other words, the alternating magnetic field that passes through the antenna coil induces a voltage that is used to operate the tag circuitry. For tags that operate in the far field region, the antennas are designed to receive TEM (transverse electric magnetic) waves and are typically a half wave-length in size.



- a) Reactive Near Field Region $< 0.62(D^3/\lambda)^{1/2}$
- b) $0.62(D^3/\lambda)^{1/2} < \text{Fresnel Region} < 2D^2/\lambda$
- c) $2D^2/\lambda < \text{Fraunhofer or Far Field Region}$

Figure 2: Field regions of a radiating element

Examples of such antennas include the printed dipole, printed folded dipole, printed inverted F (PIFA), and the patch antenna [9]. Typically, these antennas are printed on flexible substrates that allow them to be attached to objects that do not have planar surfaces.

Modulation Circuitry Most RF tags use a type of load modulation to encode the signal that is detected at the reader [1]. A resistive or reactive load, denoted as Z_{mod} in Figure 1b, is switched in and out of the circuit to achieve amplitude or phase modulation of the backscattered signal. If the tag operates in the near field of the reader, Z_{mod} is used to tune and de-tune a resonant circuit. If the tag operates in the far field of the reader, the tag switches Z_{mod} in and out of the circuit to reflect pulses back to the reader. In some cases, the load is modulated at a sufficiently high frequency to create a subcarrier that is detected at the reader. Due to the frequency separation of the carrier and subcarrier frequencies, the modulated subcarrier can be easily filtered and detected [1].

It is important to note that the wireless communication between the reader and the tag in the near field region is fundamentally different of that when the tag is in the far field region. When a tag operates in the near field of the reader, the fields emanating from the reader

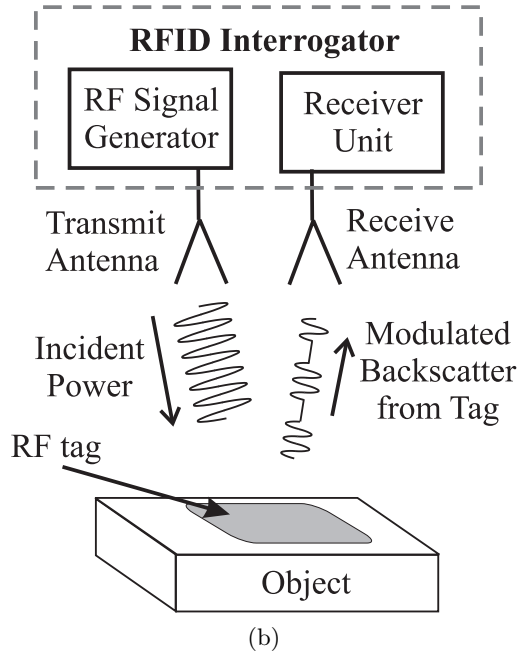
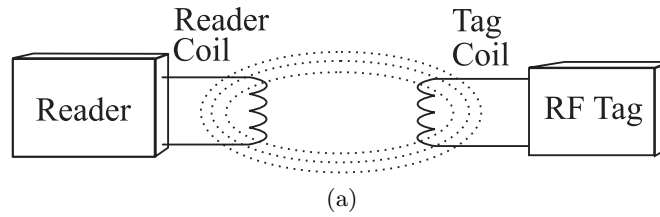


Figure 3: (a) Near field inductive coupling RF tag system communication and (b) far-field backscatter RF tag system communication

remain coupled to the reader antenna. Because of this, the link coupling the reader to the tag is similar to that of a transformer as shown in Figure 3a [1]. Therefore, if the tag changes its complex impedance through load modulation, the reader will detect a corresponding change in the impedance of its coil antenna. However, in the far field, the fields radiating from the reader are no longer coupled to the reader antenna. Instead, these fields are self-sustaining TEM fields. For the tag to communicate with the reader, the radiated fields must be reflected, or backscattered, back to the reader as shown in Figure 3b [1].

1.2.3 Tag Operating Frequencies

In order to avoid interference with other radio systems, the available frequencies for RF tag systems are governed by the Federal Communications Commission (FCC). RF tag systems typically use the unlicensed industrial, scientific, and medical (ISM) frequency bands. Since the RF tag systems are intentional radiators, they fall under the rules of the Code of Federal

Regulations, Title 47, Part 15. Common frequencies used for RF tag systems are those shown in Table 1 [1].

Available ISM Band RF Tag System Operating Frequencies		
<i>kHz</i>	<i>MHz</i>	<i>GHz</i>
< 135	6.78, 13.56, 27.125, 40.68, 915	2.45, 5.8, 24.125

Table 1: ISM band frequencies available for RF tag system use

CHAPTER II

CURRENT RF TAG CHALLENGES AND RESEARCH

As discussed in Section 1.1, Wal-mart and the Department of Defense, along with many other entities, desire to label and track individual items in their inventory. However, the relative high cost and poor performance of RF tags limit their use to tracking large items. For RF tags to be used on low cost, mass produced goods, much research is needed to lower tag cost, reduce the tag footprint, and improve the tag performance and reliability. This chapter discusses these technical challenges and current research that is being conducted to solve these problems.

2.1 Tag Cost

The cost of an RF tag consists of two primary components: the cost of the integrated circuit and the cost of the tag antenna and substrate. To reduce these costs, research is being conducted at Georgia Tech to explore the use of organic semiconductors and new, low-cost antenna manufacturing techniques on flexible substrates.

The silicon integrated circuits used in most RF tags today require relatively expensive manufacturing processes that place a barrier on the minimum cost of the chip. These processes include the growth of high quality crystalline silicon, a photolithographic process to create the integrated circuit (IC), packaging of the IC, and attachment of the IC the circuit to a board. The rapidly advancing field of organic semiconductor devices offers a low-cost alternative to these traditional silicon-based ICs. The greatest advantage of organic semiconductors is their ease of fabrication, as many organic materials can be processed at room temperature and do not require photolithography [13]. For example, Baude, et. al. [10], have prototyped a passive, 1-bit RFID transponder using organic (pentacene) semiconductors that were patterned with shadow mask techniques while keeping the substrate nominally at room temperature. Their transponder is powered through inductive coupling and consists of a 7-stage ring oscillator. These researchers report successful operation of the transponder from 125 kHz to 6.5 MHz. These authors have also demonstrated an 8-bit version of this same transponder [11] . This

transponder was successfully demonstrated at 1.19 MHz at a read distance of 1 cm.

Research is also being conducted on new methods for constructing RF tag antennas. Professor Bernard Kippelen and Andreas Haldi have prototyped several printed, flexible antennas on Polyethylene Terephthalate (PET) substrates. These prototype antennas use low cost, wet deposition techniques to deposit silver and copper onto the substrates. For more information, see Section 3.2.1.4.

2.2 Tag Footprint

Research efforts to decrease the RF tag footprint are focused on the tag antenna, which is the largest object on an RF tag. For far field RF tags, the size of the antenna is governed by the operating frequency and antenna topology. Since the frequency of operation is determined by government regulations, improved antenna topologies offer the greatest potential for size reduction.

Proposed topologies for far field RF tag antennas are the dipole, folded dipole, patch, and inverted-f (IFA) antenna. Recent RF tag antenna designs have focused on modifying these traditional antenna topologies by folding and using computer analysis to minimize resonant lengths. Recently, Li, et. al. [14], demonstrated a folded, shorted-patch antenna that can be integrated into an RF circuit board. Two implementations of this design were demonstrated. The first was constructed on an LTCC (low temperature co-fired ceramic) multilayer board with a resonant frequency of 6.36 GHz. At this frequency, antenna dimensions were $\lambda_o/16$ with a radiation efficiency of 35%. The second antenna was implemented on a RT/Duroid 5880 board with a resonant frequency of 1 GHz. The electrical length of the antenna was $\lambda_o/10$ with a radiation efficiency of 45%. In addition, Marrocco has investigated the design of uniform and non-uniform meander line antennas optimized by a genetic algorithm [15]. Keskilammi, et. al. [16], have demonstrated a unique application of these antennas by using printed text on the RFID tag as a meander line antenna.

2.3 Tag Performance

The two most important metrics of RF tag performance are the maximum read range and the reliability of communication, shown in Figure 4. These metrics are strongly affected by both the performance of the integrated circuit and the performance of the tag antenna. The

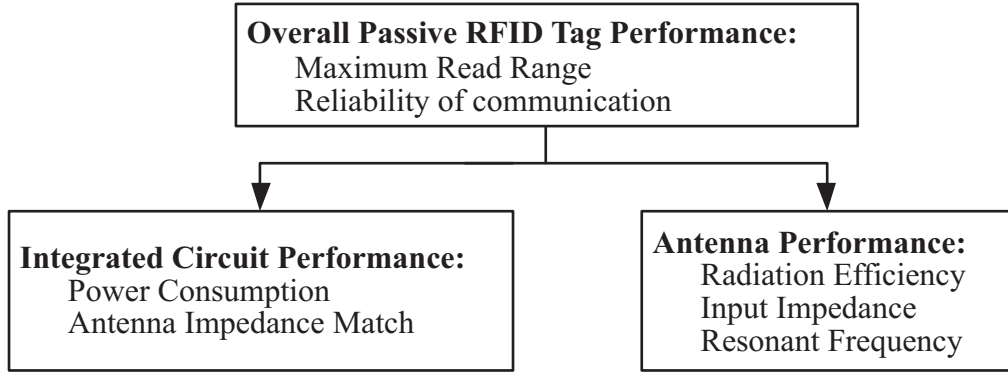


Figure 4: Passive RF tag performance metrics

power consumption by an RF tag IC is directly related to the read range. In an effort to reduce the power consumption of the IC and thus increase the read range, Karthaus and Fischer demonstrated a passive RFID transponder implemented with 0.5- μm CMOS technology that is capable of operating in the ultra high frequency (UHF) band with a projected range of 9.5m [17]. This transponder consumes 16.7 μW of power and employs phase shift keying (PSK) backscatter modulation.

The antenna performance metrics, listed in Figure 4, are affected by deformation of the antenna, polarization mismatch, the electromagnetic (EM) properties of the material to which the antenna is attached, and the EM properties and proximity of other nearby objects, which are summarized in Table 2. Therefore, a tag antenna designed to operate in a particular

Physical Causes of Antenna Performance Degradation
Antenna deformation
Polarization mismatch
EM properties of the tagged object
EM properties and proximity of nearby objects

Table 2: Physical causes of RF tag antenna performance degradation

environment will suffer performance degradation when placed in an environment other than that for which it was designed. For a passive tag, this can be particularly damaging since both the capability of the antenna to couple power into the tag circuitry and the capability of the antenna to backscatter the modulated signal will be reduced.

Several researchers have identified and investigated these issues. Siden, et. al. [18], have

investigated the effects of antenna bending through a series of simulations of a folded dipole bent at different locations along its major length. The author's simulations show how the antenna pattern and input impedance vary with bending and they relate these parameters to the RFID tag maximum read range. Foster and Burberry demonstrated measurements of omnidirectional antenna patterns in close proximity to a cylindrical metal can, bottles of water (both glass and plastic), waxed cartons of liquid, and apples [19]. In addition, it is experimentally shown that the input impedance of the antenna changes when placed in close proximity to a metal can and that the resonant frequency can change when the antenna is close to a dielectric (in this case, a plastic bottle of water).

Other researchers have proposed antenna solutions to solve some of these issues. Ukkonen, et. al., have demonstrated an IFA (inverted-f antenna) for RFID tags attached to conductive surfaces [20]. The prototyped IFA antennas showed little performance degradation when applied to a metal surface. In some cases, the IFA antennas even benefited from the power reflected from the surface. Ukkonen, et. al., have also investigated the use of an electronic band gap (EGB) ground plane to improve the performance of a patch antenna when attached to a conductive surface [21]. The paper demonstrates nominal improvement in the antenna performance. Although these antennas offer improved performance when attached to conductive materials, their drawback is increased manufacturing complexity, which will likely lead to higher manufacturing costs.

CHAPTER III

THE RADIO ASSAY

3.1 The Radio Assay Defined

As discussed in Chapter 2, current research in RF tags is focused on methods to reduce tag cost, to reduce the tag footprint, and to improve the tag performance. The research presented in this report, seeks to contribute to these research efforts by designing and building a radio assay for the study of RF tag performance. The term assay is taken from chemistry and refers to a series of tests applied to an unknown material in order to determine its properties. Hence, the radio assay is a series of tests applied to RF tag antennas to determine their performance characteristics. With only slight modifications to the setup, the radio assay will allow the following studies to be conducted:

- RF tag antenna performance in the presence of nearby objects with various electromagnetic properties
- RF tag antenna performance when attached to objects with varying electromagnetic properties
- RF tag antenna performance as a function of antenna deformation
- RF tag antenna performance as a function of antenna material and fabrication
- Optimal RF tag reader antenna topologies
- RF tag antenna diversity experiments
- Characterization of small-scale fading in RF tag systems

Since the scope of these experiments is quite broad, the following two radio assay experiments were chosen to be presented in this report:

- RF tag antenna performance when attached to objects with varying electromagnetic properties

- RF tag antenna performance as a function of antenna material and fabrication

These two experiments seek answers to the following questions:

What is the decrease in gain and radiation efficiency of the RF tag antenna when attached to different materials?

Can RF tag antenna performance be improved by tuning the impedance match of the antenna for each material to which the tag antenna is attached?

What is the penalty, in terms of antenna gain, that is incurred by using low cost alternatives to standard RF tag antennas?

The results of these experiments are presented in Chapter 5.

3.2 General Equipment for the Radio Assay

Although the required equipment for the radio assay may vary for each particular experiment, the following basic devices are essential for each. These devices are as follows:

- RF tag antenna
- Transmission line topology transformer
- Balun
- Tunable impedance transformation network
- Directional antennas
- Antenna range

This remainder of this chapter discusses the purpose, operation, and specific implementation of these devices for the radio assay. The particular methods and modifications used for the experiments presented in this report may be found in Chapter 4.

3.2.1 RF Tag Antenna

3.2.1.1 Antenna Selection

As discussed in Section 1.2.2.2, common antennas for tags that operate in the far field of the reader include the printed dipole, printed folded dipole, printed inverted F (PIFA), and patch

antenna. The PIFA and patch antenna are relatively difficult to construct since both use a conductor that is suspended above a ground plane. In contrast, both the printed dipole and printed folded dipole are planar structures that can be easily constructed on flexible substrates. Hence, the printed dipole and printed folded dipole were chosen over the PIFA and patch antennas. Furthermore, the input impedance of an ideal, half-wave dipole with a sinusoidal current distribution, is 73Ω while the input impedance of a similarly fed printed folded dipole is approximately 292Ω . On a thin plastic substrate, these antennas are fed using a coplanar strip (CPS) transmission line. The impedance of a CPS transmission line, illustrated in Figure 5, is proportional to the distance between the strips (d), the width of the strips (w), and the relative permittivity of the substrate. Using the design formulas given by Wadell [22], it was

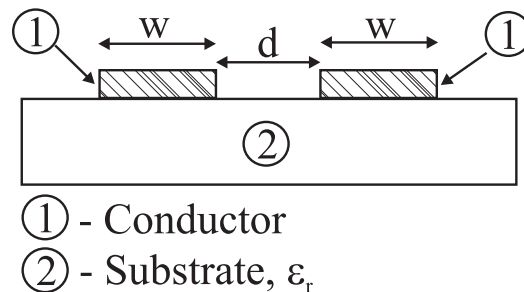


Figure 5: Cross section of coplanar strip (CPS) transmission line

found that the dimensions of the CPS line required to achieve an impedance match with the printed dipole (73Ω) were not practical since the required d was less than 1 mm. However, an impedance match with the printed folded dipole required the dimensions d and w to be only a few millimeters. Therefore, the printed folded dipole was chosen to be the prototype RF tag antenna in the radio assay experiments.

3.2.1.2 Printed Folded Dipole Theory

According to Stutzman and Thiele [12], the folded dipole antenna operates as an unbalanced, radiating transmission line. The far field pattern of the half wave-length folded dipole is the same as that of a dipole antenna, however as mentioned previously, the folded dipole has an input impedance that is approximately 4 times that of a dipole. The following derivation, described by Stutzman and Thiele [12], explains the operation of the folded dipole by decomposing the current distribution into a transmission line mode and an antenna mode, shown in Figure 6. The superposition of the transmission line mode current, I_{trans} , and the antenna mode current,

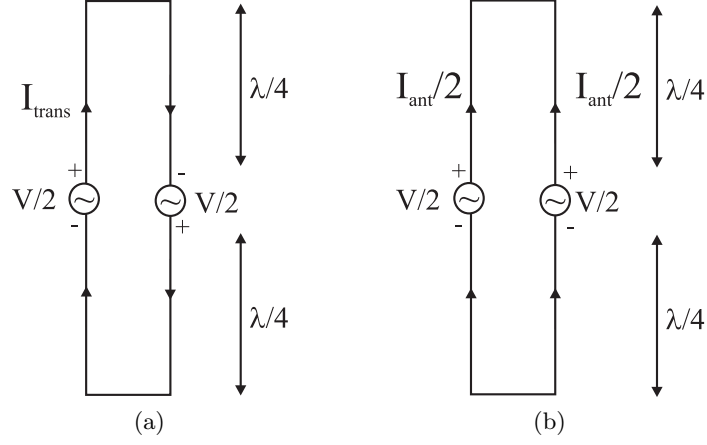


Figure 6: Folded dipole decomposed into the (a) transmission line mode and (b) antenna mode for impedance analysis

I_{ant} , represent the total current feeding the folded dipole. In the transmission line mode, the currents in each arm of the folded dipole are 180° out of phase and closely spaced. Therefore, these currents cancel and do not contribute to the far field radiation of the antenna. The input impedance of the transmission line mode is that of a short circuit transmission line. From (14) in Section 3.2.3.1, the input impedance of a short circuit transmission line is given as follows:

$$\begin{aligned}
 \tilde{Z}_{trans}(l) &= Z_o \frac{(\tilde{Z}_{load} + jZ_o \tan(\beta l))}{(Z_o + j\tilde{Z}_{load} \tan(\beta l))} \\
 &= Z_o \frac{jZ_o \tan(\beta l)}{Z_o} \quad \text{since } \tilde{Z}_{load} = 0 \\
 &= jZ_o \tan(\beta l)
 \end{aligned} \tag{3}$$

In contrast with the transmission line mode currents, the antenna mode currents reinforce and contribute to the far field radiation. Just as the currents of the folded dipole can be decomposed into two modes, the feed voltages associated with these currents can be divided as shown in Figure 6. In the antenna mode, since no current travels around each end of the folded dipole, the folded dipole can be divided into two linear dipoles with equal currents, $I_{ant}/2$. If the two modes are summed, the total input current to the folded dipole is $I_{trans} + I_{ant}/2$. From this, the input impedance of the folded dipole is

$$\begin{aligned}
 Z_{in} &= \frac{V_{tot}}{I_{tot}} \\
 &= \frac{V/2 + V/2}{I_{trans} + I_{ant}/2} \\
 &= \frac{V}{I_{trans} + I_{ant}/2}
 \end{aligned} \tag{4}$$

Since $I_{trans} = \frac{V}{2\tilde{Z}_{trans}}$ and $\frac{I_{ant}}{2} = \frac{V}{2\tilde{Z}_{dip}}$

the input impedance (4), becomes

$$Z_{in} = \frac{4\tilde{Z}_{trans}\tilde{Z}_{dip}}{2\tilde{Z}_{trans} + 2\tilde{Z}_{dip}} \quad (5)$$

If in (3), $l = \lambda/4$, then $\tilde{Z}_{trans} = \infty$ and the input impedance of the folded dipole (5), reduces to $Z_{in} = 4\tilde{Z}_{dip}$ as stated.

3.2.1.3 Printed Folded Dipole Design

Design equations for the printed folded dipole are presented by Lampe [23]. These equations, along with Figure 7.71 and Equation 7.71 from Elliott [24], were used to design the printed folded dipole for the desired input impedance of 233Ω at 915 MHz. These equations provided only an estimate of the real part of the input impedance. A numerical simulation would be required in order to obtain an exact value. However, since this antenna was intended for use with a tunable impedance transformation network, exact input impedance calculations were not required. The dimensions of the printed folded dipole used for the radio assay are given in Figure 7.

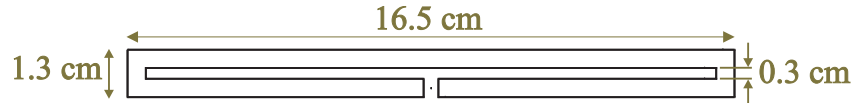


Figure 7: Printed folded dipole dimensions for 915MHz

3.2.1.4 Printed Folded Dipole Construction

The design formulas for the input impedance of the folded dipole assume that the antenna is constructed of a good conductor. However, this assumption is not valid for the printed folded dipoles used in the radio assay. These folded dipoles have a thickness that is less than the skin depth, the conductor is not uniformly distributed, and the Ohmic losses vary from antenna to antenna. As a result, the input impedance of the printed folded dipoles is expected to differ from the theoretical value and is expected to vary from antenna to antenna. Three low-cost prototype RF tag antennas made using different manufacturing methods were provided by Andreas Haldi and Professor Bernard Kippelen and are shown in Figures 9-11. These antennas

include an electroless silver antenna, electroless copper antenna, and an indium tin oxide (ITO) antenna. Each of these antennas were deposited on flexible, polyethylene terephthalate (PET) substrates.

The electroless silver and copper antennas were made by printing a mask of the antenna outline on a PET substrate that was coated with an adhesion layer for laser printer toner. The printing was done with a standard laser printer. The printed substrates were then placed in solutions where a reduction reaction was triggered to deposit the silver and copper films onto the substrate. The chemicals used for this process were the HE-300 solution by Peacock Laboratories, Inc. for the silver films and the Circuposit Electroless Copper 3350 by Shipley, for copper films. Once the metal films were deposited, the antennas were dried in a vacuum oven and then in placed in an ultrasonic acetone bath to lift the printed mask (and the metal adhering to it) off of the substrate as shown in Figure 8. After the mask was removed, only the metal film antenna remained. The cost of manufacturing the electroless silver and electroless

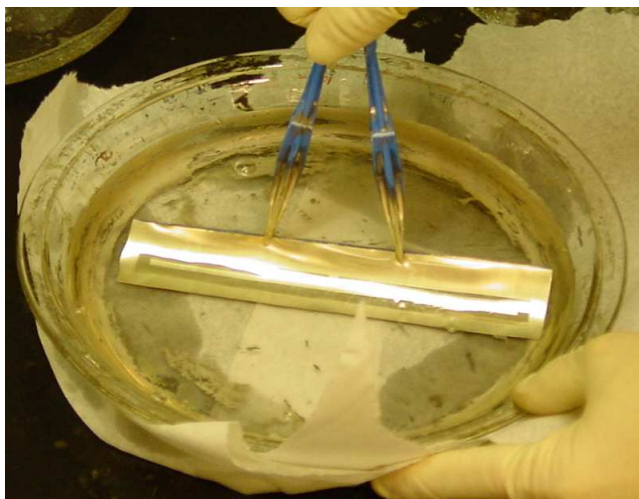


Figure 8: 915 MHz electroless silver flexible folded dipole in acetone bath to remove printed mask

copper antennas was approximately one dollar per antenna. This cost only reflects the expense of purchasing the chemical solutions in small quantities. The cost of mass producing these antennas is expected to be significantly less.

The ITO antenna was made by etching the antenna geometry from a 7 mil ITO coated PET substrate purchased from Sheldal. The etchant was a 5:5:1 mixture of hydrochloric acid, deionized water, and sulfuric acid. This antenna is unique in that it is optically transparent.

RF Tag Antennas					
	<i>Conductor Material</i>	<i>Antenna Substrate</i>	<i>Conductor Thickness</i>	<i>Bulk Conductivity</i>	<i>DC Resistance</i>
Baseline	1 oz. Copper	Rigid FR4	35.5 μm	5.7x10 ⁷ * S/m	0 Ω
Silver	Electroless Silver	Flexible PET**	202 \pm 19nm	8.9x10 ⁶ *** S/m	36 Ω
Copper	Electroless Copper	Flexible PET	195 \pm 17nm	6.8x10 ⁶ *** S/m	49 Ω
ITO	Indium Tin Oxide	Flexible PET	1 μm	1.6x10 ⁴ *** S/m	4K Ω

*Value from Stutzman and Thiele [12]

**PET - Polyethylene Terephthalate

***Estimated value calculated from the DC resistance and antenna geometry

Table 3: RF tag antenna physical characteristics

In addition, a baseline antenna was milled by Bob House on 1 oz. copper-clad FR4 as shown in Figure 12. This antenna was used as a point of comparison to evaluate the performance of the flexible antennas. The characteristics of each antenna are shown in Table 3. For the remainder of this report, the electroless silver, electroless copper, the indium tin oxide, and the copper-clad FR4 antennas will be referred to as simply the silver, copper, ITO and baseline antennas, respectively.



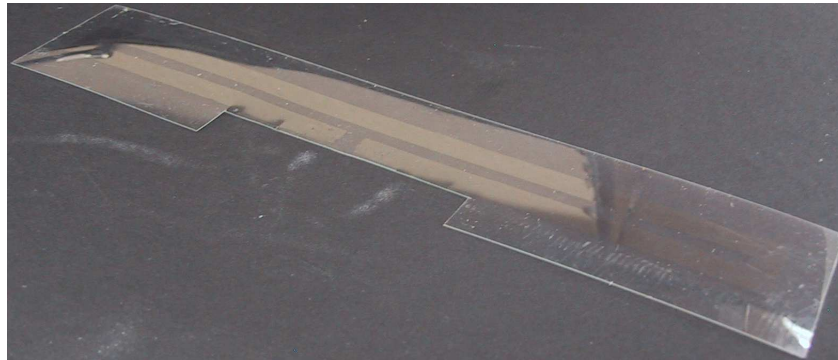
Figure 9: Flexible 915 MHz folded dipole made from electroless silver deposited on a PET substrate

3.2.2 Balun and Transmission Line Topology Transformer

When a balanced system is connected to an un-balanced system, care must be taken to ensure that the proper relationship between the currents is maintained. In a balanced system, the



(a)



(b)

Figure 10: Transparent and flexible 915 MHz folded dipole antenna made from indium tin oxide (ITO) deposited on a PET substrate

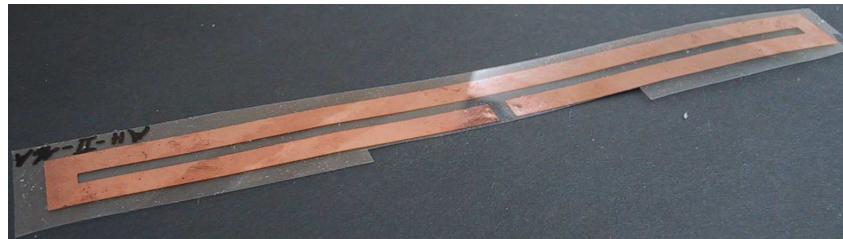


Figure 11: Flexible electroless copper 915 MHz folded dipole deposited on a PET substrate

voltages on the conductors are referenced to a common reference plane. For example, the coaxial line in Figure 13a is an unbalanced system. In a balanced system, a differential voltage is maintained between the conductors without reference to a common plane. An example of such a system is the folded dipole shown in Figure 13b. In each of these systems, the forward and return currents, I_a and I_b respectively, are equal in magnitude and 180° out of phase. When the two systems are connected, this current balance must not be disturbed; otherwise, spurious lobes will appear the far field radiation pattern. For the case of a coaxial line connected to a folded dipole, the current balance is disturbed when the return current from the folded dipole, I_b , divides into I_{outside} and I_{inside} which flow on the outside and inside of the coaxial feed line

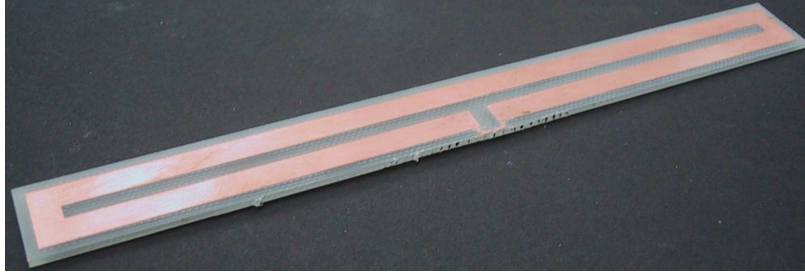


Figure 12: Rigid baseline 915 MHz folded dipole milled on copper-clad FR4 substrate

shield as shown in Figure 13c. The reason that the outside and inside of the shield act as two independent current paths is because the thickness of the shield is much larger than that of the skin depth at RF and microwave frequencies.

To prevent this from occurring, a balun (formed from the words BALanced to UN-balanced) may be used to connect the unbalanced coaxial line to the balanced folded dipole antenna. A balun is a device that transforms an unbalanced signal into a balanced signal without disturbing the current relationship. Many different balun designs are available that offer varying bandwidths and impedance ratios in a variety of transmission line topologies. In general, as the bandwidth of the balun increases, so does the complexity. Therefore, since the radio assay experiments presented in this report are narrow-band, a simple quarter wave balun was chosen to feed the RF tag antenna.

The quarter wave balun consists of quarter wave-length section of transmission line, or balancing line, that is attached to the outside of the coaxial feed line as shown in Figure 14. The center conductor of the coaxial feed line is connected to the shield of the balancing line via connection 1 and the shields of the balancing line and the coaxial feed line are shorted at 2. The equivalent circuit of this balun is described by Riddle [25], shown in Figure 15. Figure 15a shows the coaxial feed line with a reference point established at point 2 which corresponds to the location of the shorted shields shown in Figure 14. The outside of the shield of the coaxial feed line is one quarter wave-length long and has a impedance of Z_{outside} which corresponds to the current path for I_{outside} . This impedance is represented in Figure 15a as a quarter wave-length transmission line connected between the shield of the coaxial feed line and ground. The inside of the coaxial feed line has an impedance of 50Ω which is shown as Z_o in Figure 15a. Z_{outside} effectively loads the return path for the return current of the folded dipole, I_b from Figure 13c,

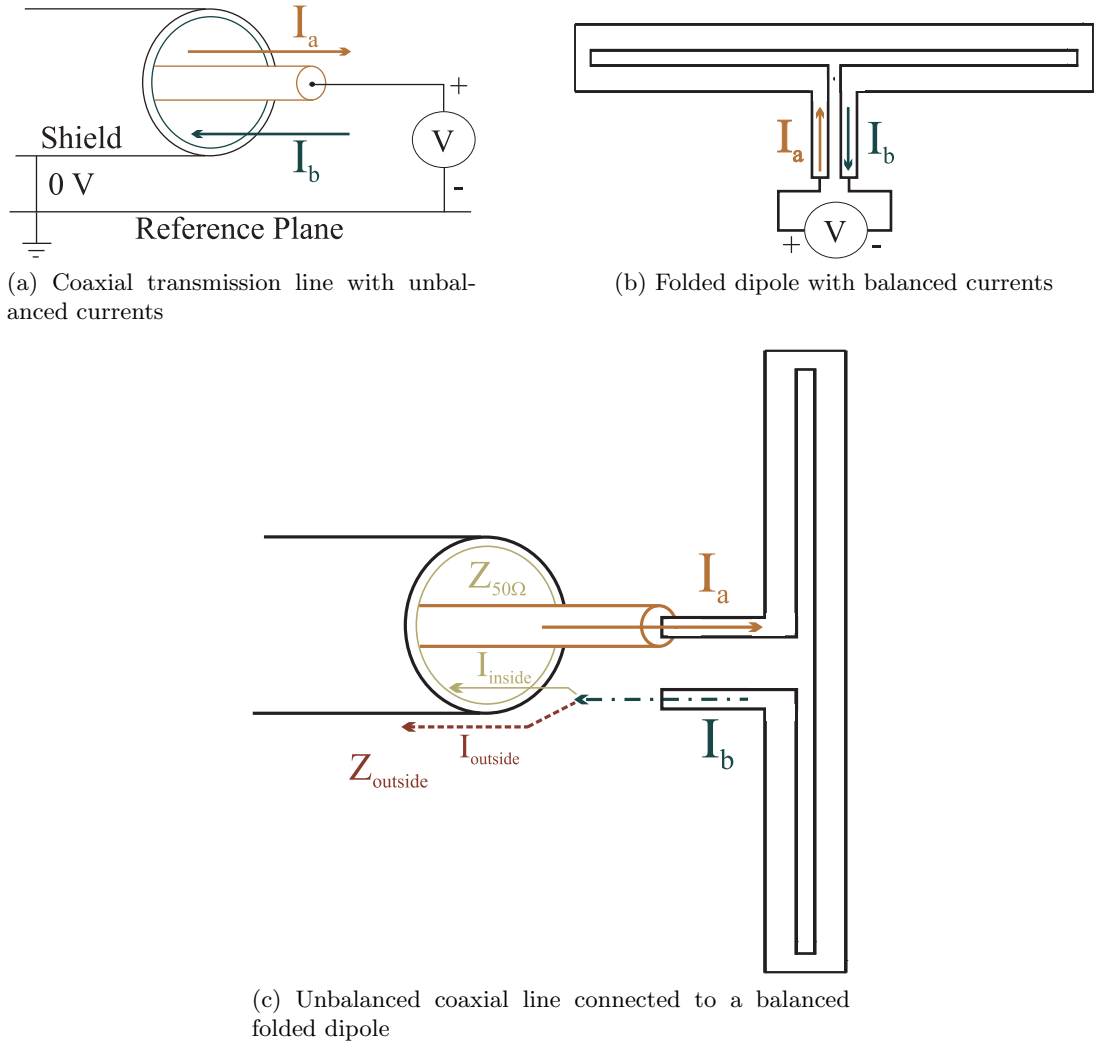


Figure 13: Balanced and unbalanced systems and their connection

disturbing the current balance and causing a common mode current to flow. The balancing line corrects this problem by equally loading the center conductor of the coaxial line for a narrow-band of frequencies centered about the design frequency. The balancing line impedance is represented in Figure 15b by a quarter wave line connected from the center conductor of the coaxial feed line to ground. Since only the shield of the balancing line is connected, it provides a load approximately equal to Z_{outside} .

A convenient way to quantify the balun performance is through use of the balun ratio. The balun ratio is similar in concept to the common mode rejection ratio (CMRR) used in amplifier design. The balun ratio, defined by Woodward and Perlow [26], is the ratio of the differential mode current to the common mode current denoted as I_a and I_b in Figure 16b. In order to determine the I_a and I_b , the board shown in Figure 16 and Figure 17 was used to

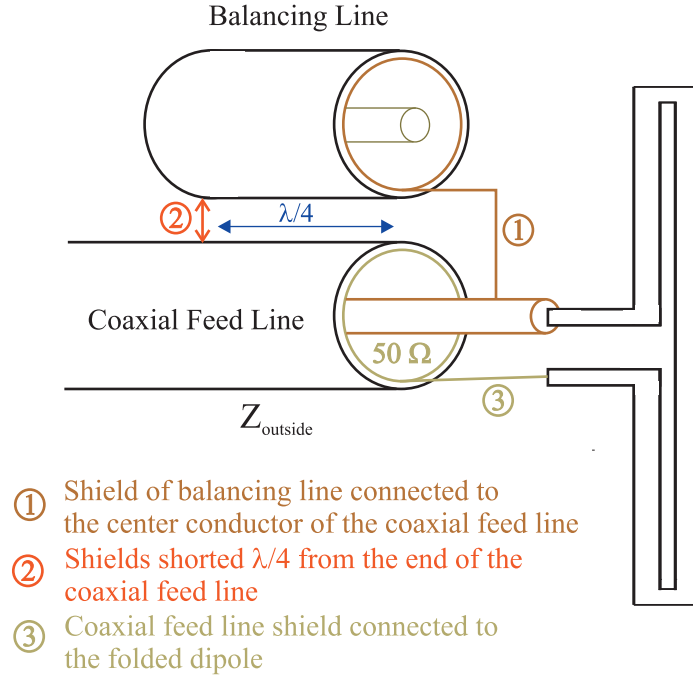
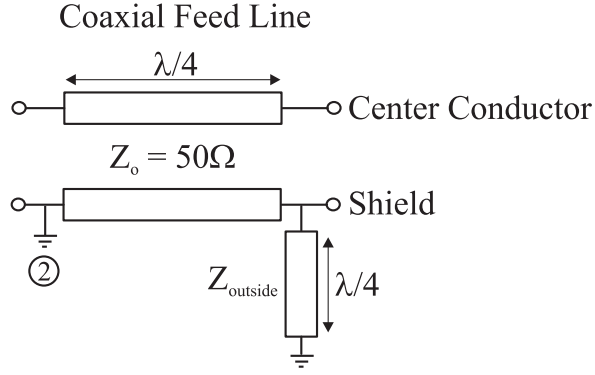
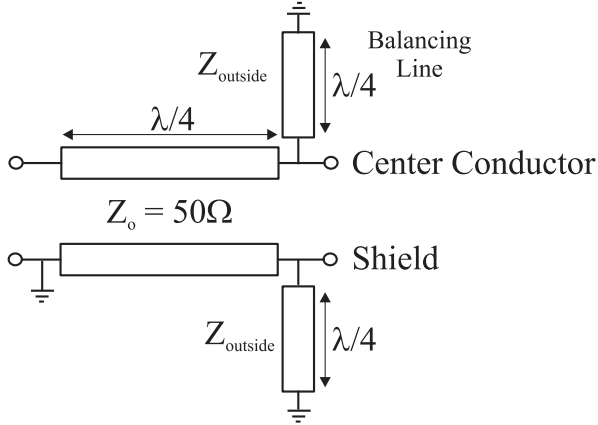


Figure 14: Quarter wave balun with folded dipole connected to the balanced terminals

measure the voltage gains from port 1 to port 2 and 3. The un-balanced terminal of the balun was connected to the input SMA connector and the balanced terminals were soldered to two, tapered microstrip transmission lines, shown in Figure 17a. The impedance of each tapered line was 25Ω to ground which provided a matched load to each of the balanced terminals of the balun. These microstrip lines were tapered to 50Ω in order for the board to be interfaced with a network analyzer. The 2-port S parameters of the balun and test board were measured using an Agilent 8753E network analyzer. First, the S parameters were measured from port 1 to port 2 with port 3 terminated in a matched load. This voltage gain was denoted as S21 and is proportional to I_1 , shown in Figure 16b. Then, this process was repeated with port 2 terminated with a matched load. This voltage gain was denoted as S31 and is proportional to I_2 as shown in Figure 16b. Woodward and Perlow [26], decompose I_1 and I_2 into the differential and common mode currents, I_a and I_b respectively. From Figure 16b, it can be seen that $I_1 = I_a + I_b$ and $I_2 = I_a - I_b$. Thus, by taking the sum and difference of I_1 and I_2 , the balun ratio



(a) Equivalent circuit of quarter wave section of coaxial feed line without balancing line attached



(b) Equivalent circuit of coaxial feed line with balancing line attached

Figure 15: Quarter wave balun equivalent circuits

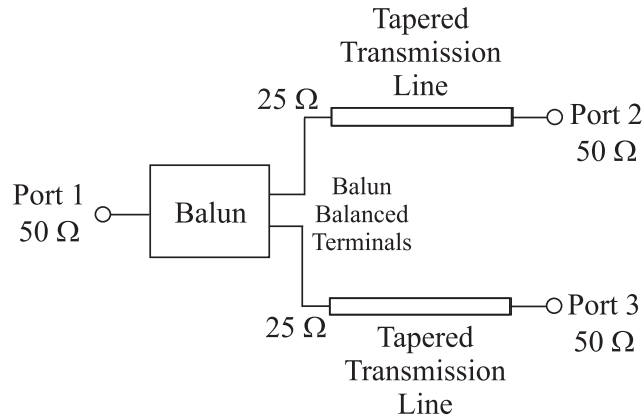
can be calculated as follows:

$$\text{Balun Ratio} = 20\log_{10} \left| \frac{I_a}{I_b} \right| \quad (6)$$

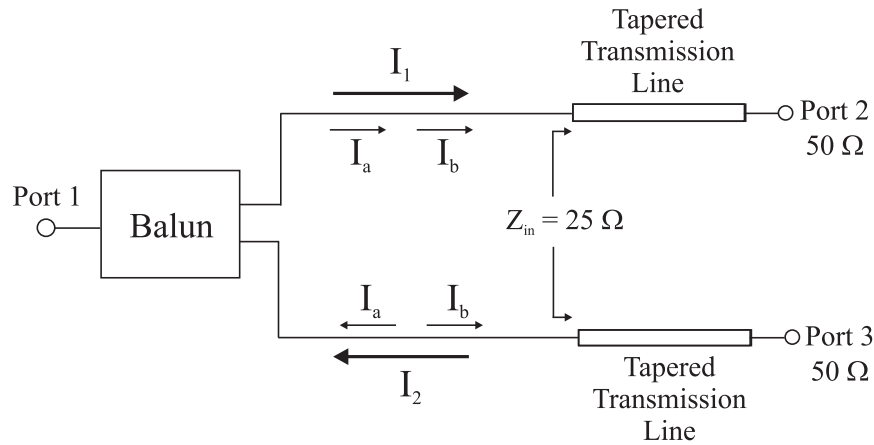
$$= 20\log_{10} \left| \frac{I_1 + I_2}{I_1 - I_2} \right| \quad (7)$$

$$= 20\log_{10} \left| \frac{S_{21} - S_{31}}{S_{21} + S_{31}} \right| \quad (8)$$

Equations (6) and (7) are presented as defined by Woodward and Perlow [26]. However, to make the balun ratio more intuitive, (8) has been modified so that the balun ratio yields the values described in the following. With reference to Figure 16b, if only a differential current is present ($I_b = 0$), $S_{21} = -S_{31}$ and the balun ratio will yield $+\infty$ dB. If only a common mode current exists ($I_a = 0$), $S_{21} = S_{31}$ and the balun ratio will be $-\infty$ dB. The measured S parameters of the quarter wave balun and the balun test board at 915 MHz are shown in Table 4. As can be seen, S11, S22, and S33 show that the balun is not matched to 50 Ω . Theoretically, since balun



(a) Equivalent circuit of balun amplitude and phase test board

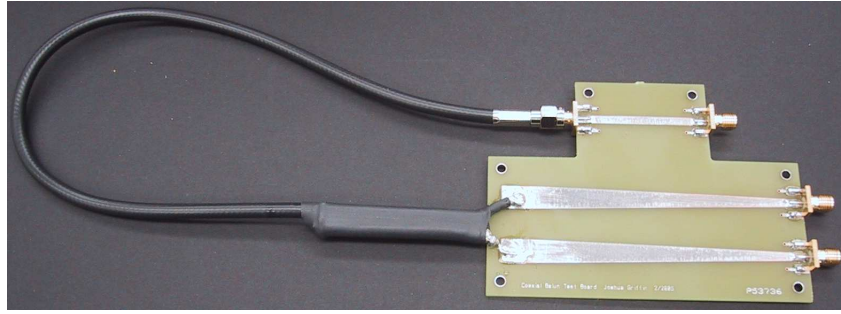


(b) Differential and common mode currents on balun amplitude and phase test board

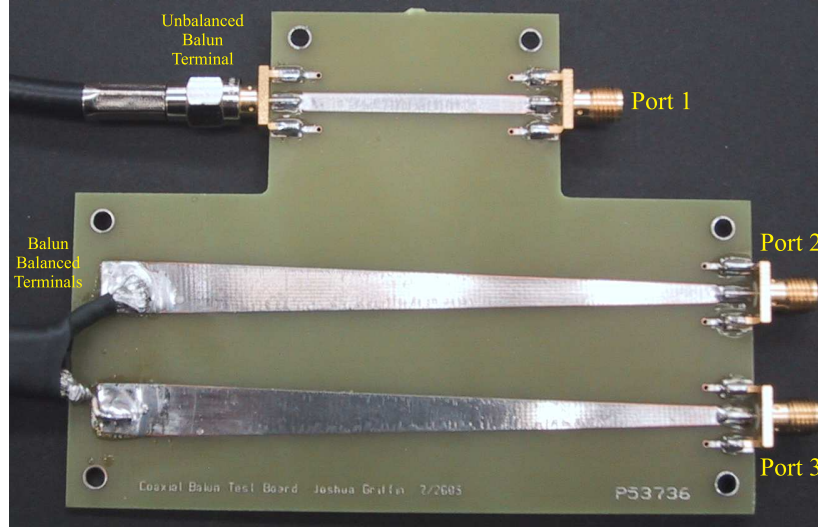
Figure 16: Equivalent circuit and currents on the balun amplitude and phase test board

design does not transform the impedance of the coaxial feed line, the impedance mismatch is likely due to manufacturing difficulties. The most likely source of this impedance mismatch is melting of the dielectric where the two shields were shorted. However, this impedance mismatch is not significant since the balun will be fed by a tunable impedance transformation network, Section 3.2.3. As can be seen in Figure 18, the quarter wave balun has a balun ratio of 35.9 dB at 915MHz. Clearly, the quarter wave balun performs optimally at 877 MHz with a balun ratio of 43 dB. The performance at 915 MHz could be improved by shortening or lengthening the quarter wave stub. However, antenna range tests showed that the current quarter wave balun performance was adequate for the experiments of the radio assay.

The loss in the quarter wave balun was measured using a back-to-back measurement. Two



(a) Balun amplitude and phase balance test board with quarter wave balun attached



(b) Balun amplitude and phase balance test board with ports labelled

Figure 17: Quarter Wave Balun and Balance Test Board

quarter wave baluns, constructed in the same manner, were connected at their balanced terminals and the two un-balanced terminals were connected to an Agilent 8753E network analyzer yielding the S parameters in Table 5. The loss of the quarter wave balun was assumed to be $1/2$ that of the back-to-back measurement, shown Figure 19. The insertion loss was calculated using the average of S_{21} and S_{12} as follows:

$$\begin{aligned} \text{I.L.} &= -20 \log |(S_{21,12\text{avg}})^{1/2}| \\ &= 0.84 \text{ dB} \end{aligned} \tag{9}$$

Quarter Wave Balun S Parameters at 915 MHz				
S_{11}	S_{21}	S_{31}	S_{22}	S_{33}
$0.575 \angle -145.0^\circ$	$0.448 \angle -164.3^\circ$	$0.453 \angle 14.0^\circ$	$0.612 \angle -38.0^\circ$	$0.597 \angle -39.5^\circ$

Table 4: Pertinent S parameters of quarter wave balun and balance test board for balun performance characterization

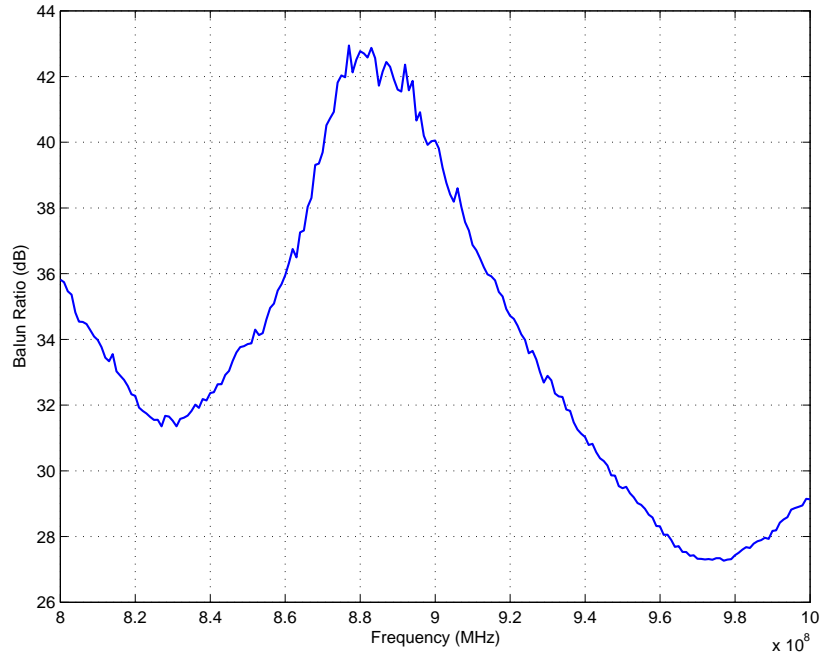


Figure 18: Balun ratio of quarter wave balun versus frequency

Back to Back Quarter Wave Balun S Parameters at 915 MHz			
S_{11}	S_{21}	S_{12}	S_{22}
0.48 \angle 76.1 $^\circ$	0.82 \angle 141 $^\circ$	0.83 \angle 142 $^\circ$	0.46 \angle 37.3 $^\circ$

Table 5: S parameters of two back-to-back quarter wave baluns

3.2.3 Tunable Impedance Transformation Network

3.2.3.1 Transmission Line Overview

In order to justify and understand the purpose of an impedance transformation network, it is necessary to have a basic understanding of transmission lines. Transmission lines are passive devices that transport electromagnetic power from one point to another, usually at a constant velocity. A transmission line consists of two conductive pathways, represented in circuit theory by an upper and lower bar, as shown is Figure 20. In the transmission line, the voltage drop across the bars and the current flowing on the bars are functions of both time and position. This gives rise to the notion of a voltage and current wave traveling through the line. The following formulas are time-harmonic, phasor solutions to the telegrapher's equations and describe the

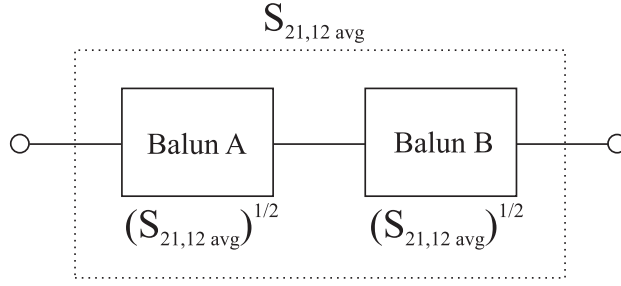


Figure 19: Diagram of back-to-back quarter wave balun measurement that shows how S21 and S12 of the back-to-back measurement were attributed equally to each balun

voltage and current waves on an arbitrary transmission line:

$$\tilde{V}(z) = \underbrace{V_o^+ e^{-j\beta z}}_{\text{Forward}} + \underbrace{V_o^- e^{j\beta z}}_{\text{Backward}} \quad (10)$$

$$\tilde{I}(z) = \underbrace{\frac{V_o^+}{Z_o} e^{-j\beta z}}_{\text{Forward}} - \underbrace{\frac{V_o^-}{Z_o} e^{j\beta z}}_{\text{Backward}} \quad (11)$$

where

- Z_o is the characteristic impedance of the transmission line

- β is the wavenumber and is equal to $\frac{2\pi}{\lambda}$

- z is the distance from the reference plane at $z = 0$. -Lossless lines have been assumed

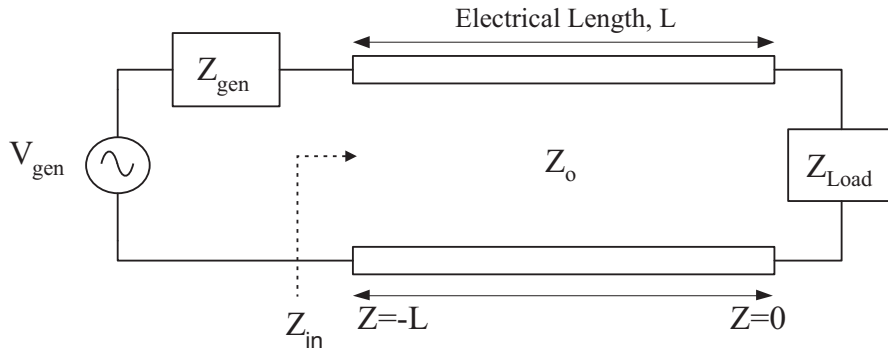


Figure 20: Arbitrary transmission line with load Z_{load} driven by a voltage source V_{gen} with an internal impedance Z_{gen}

From (10) and (11), the voltage and current at any point in the transmission line are the sum of the forward and backward propagating waves. The ratio of the voltage and current on the transmission line is the characteristic impedance, Z_o . However, at the terminations of the line,

the ratio of the voltage and current waves must be that of the load (or generator) impedance. If the characteristic impedance of the line is mismatched with the load impedance, a backward propagating, or reflected, wave is generated to maintain this constraint throughout the line. As expected, the magnitude of the reflected wave is proportional to the impedance mismatch and is described by the reflection coefficient, which is the ratio of the reflected and forward propagating waves.

$$\tilde{\Gamma}_{load} = \frac{V_o^-}{V_o^+} = \frac{\tilde{Z}_{load} - Z_o}{\tilde{Z}_{load} + Z_o} \quad (12)$$

From (12), it can be seen that if the load impedance is equal to the characteristic impedance, no reflected wave is generated. Typically, this matched condition is desired so that no power is reflected from the load. Instead, when a lossless transmission line is matched, all of the power traveling in the transmission line is absorbed by the load.

It is often useful to calculate an equivalent impedance that accounts for any mismatch between the load and characteristic impedance of the line, Z_o . This impedance is found by substituting (12) into (10) and (11) and then taking their ratio [27].

$$\begin{aligned} \tilde{Z}(z) &= \frac{\tilde{V}(z)}{\tilde{I}(z)} \\ &= \frac{V_o^+ (e^{+j\beta z} + \tilde{\Gamma}_{load} e^{-j\beta z})}{\frac{V_o^+}{Z_o} (e^{+j\beta z} - \tilde{\Gamma}_{load} e^{-j\beta z})} \\ &= Z_o \frac{e^{+j\beta z} + \tilde{\Gamma}_{load} e^{-j\beta z}}{e^{+j\beta z} - \tilde{\Gamma}_{load} e^{-j\beta z}} \end{aligned} \quad (13)$$

From (13), it can be seen that this equivalent impedance, $\tilde{Z}(z)$, accounts for the mismatch between the line and the load. In effect, this formula transforms the load impedance into an equivalent impedance that is a distance z away from the reference plane ($z=0$). This equation can be put into a more useful form as given by Pozar [27]:

$$\begin{aligned} \tilde{Z}(z) &= Z_o \frac{(Z_o + \tilde{Z}_{load})e^{+j\beta z} + (\tilde{Z}_{load} - Z_o)e^{-j\beta z}}{(Z_o + \tilde{Z}_{load})e^{+j\beta z} - (\tilde{Z}_{load} - Z_o)e^{-j\beta z}} \\ &= Z_o \frac{Z_o e^{+j\beta z} + \tilde{Z}_{load} e^{+j\beta z} - Z_o e^{-j\beta z} + \tilde{Z}_{load} e^{-j\beta z}}{Z_o e^{+j\beta z} + \tilde{Z}_{load} e^{+j\beta z} + Z_o e^{-j\beta z} - \tilde{Z}_{load} e^{-j\beta z}} \\ &= Z_o \frac{2\tilde{Z}_{load} \cos(\beta z) + j2Z_o \sin(\beta z)}{2Z_o \cos(\beta z) + j2\tilde{Z}_{load} \sin(\beta z)} \\ &= Z_o \frac{(\tilde{Z}_{load} + jZ_o \tan(\beta z))}{(Z_o + j\tilde{Z}_{load} \tan(\beta z))} \end{aligned} \quad (14)$$

Using this formula, the arbitrary transmission line, shown in Figure 20, can be reduced to the following equivalent circuit as shown in Figure 21, where \tilde{Z}_{in} is given as

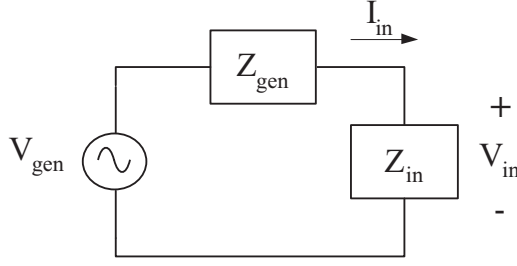


Figure 21: Equivalent circuit of an arbitrary transmission line with input impedance Z_{in} driven by a voltage source V_{gen} with an internal impedance Z_{gen}

$$\tilde{Z}_{in} = \tilde{Z}(l) = Z_o \frac{(\tilde{Z}_{load} + jZ_o \tan(\beta l))}{(Z_o + j\tilde{Z}_{load} \tan(\beta l))} \quad (15)$$

This representation of the arbitrary line, which accounts for the load mismatch, allows the time averaged power delivered to the load to be calculated as demonstrated by Pozar [27].

$$\begin{aligned} P_{avg-load} &= \frac{1}{2} \text{Re}\{\tilde{V}_{in} \tilde{I}_{in}^*\} \\ &= \frac{1}{2} \text{Re}\{\tilde{V}_{in} \frac{\tilde{V}_{in}^*}{\tilde{Z}_{in}}\} \\ &= \frac{1}{2} |\tilde{V}_{in}|^2 \text{Re}\left\{\frac{1}{\tilde{Z}_{in}}\right\} \\ &= \frac{1}{2} \left| \frac{\tilde{V}_{gen} \tilde{Z}_{in}}{\tilde{Z}_{in} + \tilde{Z}_{gen}} \right|^2 \text{Re}\left\{\frac{1}{\tilde{Z}_{in}}\right\} \end{aligned} \quad (16)$$

Since the transmission line is lossless and both the generator and load mismatches have been accounted for, all of the power traveling in the line will be delivered to the load. This holds even if the signal must pass through multiple, cascaded, mismatched transmission lines. To show this, consider two cascaded, arbitrary transmission lines connecting a generator and a load, shown in Figure 22. Using (14), Z_{load} and Z_b can be reduced to Z_{in-b} as illustrated in Figure 23. Then, using the same procedure, Z_{in-b} and Z_a can be reduced to Z_{in-a} , shown in Figure 24. The power delivered to the equivalent load Z_{in-a} , can be calculated using (16). Since the transmission lines are both lossless and Z_{in-a} accounts for the mismatches between Line A, Line B, and the load, the power delivered to Z_{in-a} is the power delivered to Z_{load}

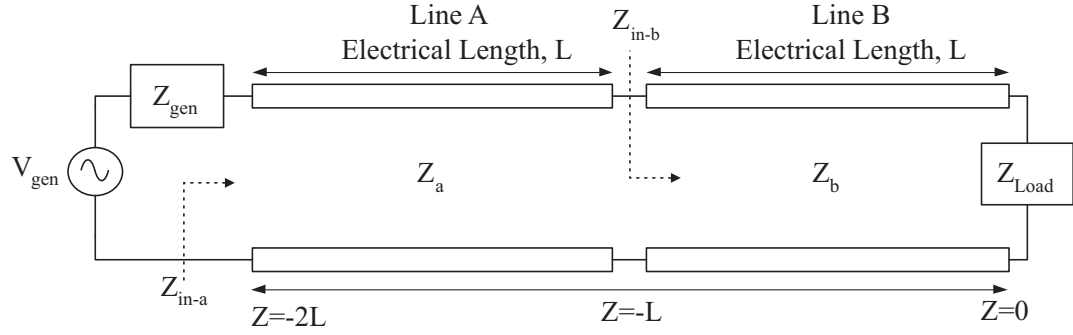


Figure 22: Equivalent circuit of two cascaded, arbitrary transmission lines of characteristic impedance Z_a and Z_b

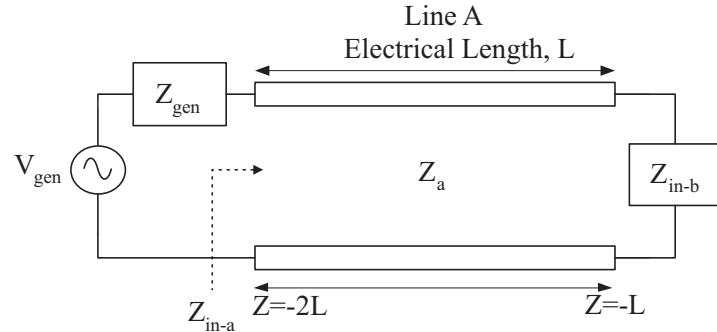


Figure 23: Equivalent circuit of transmissions line shown in Figure 22 with Z_b and Z_{load} reduced to Z_{in-b}

The case of cascaded, mismatched lines occurs commonly in many actual systems. One such example is an antenna feed in which the antenna, balun, and signal source are not matched. In such a case, it is desirable to transfer the maximum power to the antenna. It can be shown that the maximum power is transferred to the load (antenna) when the equivalent input impedance is the complex conjugate of the generator impedance, $\tilde{Z}_{gen} = \tilde{Z}_{in}^*$ [27].

3.2.3.2 Impedance Matching Network

The goal of an impedance matching network is to enforce $\tilde{Z}_{in-A} = \tilde{Z}_a^*$ and $\tilde{Z}_{in-B} = \tilde{Z}_b^*$, as shown in Figure 25. In other words, the matching network must provide a conjugate match to both the load and generator impedance. As discussed in Section 3.2.3.1, a conjugate match allows maximum power to be delivered to the load. Several types of impedance matching networks are commonly realized using lumped elements, tuning stubs, and tapered transmission lines. Lumped element and tuning stub networks both use reactive elements to transform the impedance. Lumped element networks are typically used up to about 1 GHz while tuning stubs

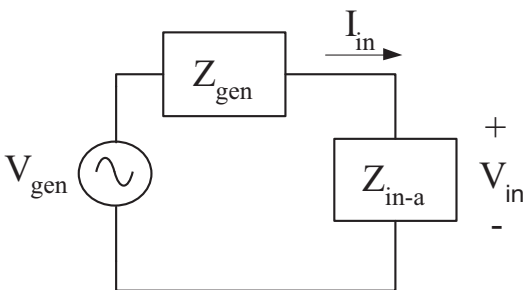


Figure 24: Equivalent circuit of transmission line shown in Figure 23 with Z_{in-b} and Z_a reduced to Z_{in-a}

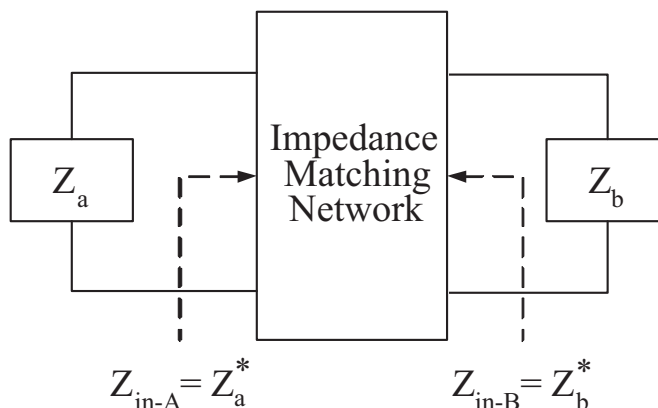


Figure 25: Diagram of general impedance matching network

and tapered lines become practical at microwave frequencies. Tapered transmission lines are based upon the theory of small reflections and use a gradual change in the impedance to achieve a match [27]. Tapered lines are usually implemented in planar transmission line topologies such as the microstrip or coplanar waveguide (CPW). Important design considerations of an impedance matching network are its matching range, bandwidth, and loss.

From circuit theory, it is possible to describe any generalized two-port network with a two-port parameter matrix. Common types of two-port network matrices are impedance, admittance, S, and ABCD parameters. From these parameters, many different equivalent circuits may be derived. Two of the most common equivalent circuits, the Pi and the T, are derived directly from the impedance and admittance parameters. If the networks are reciprocal and lossless, the components in these equivalent circuits, shown in Figure 26, are purely imaginary [27]. In Figure 26, the component values are given as $Z = R + jX$ and $Y = G + jB$. Therefore, for the special case of reciprocal, lossless networks, the components of T and Pi networks may

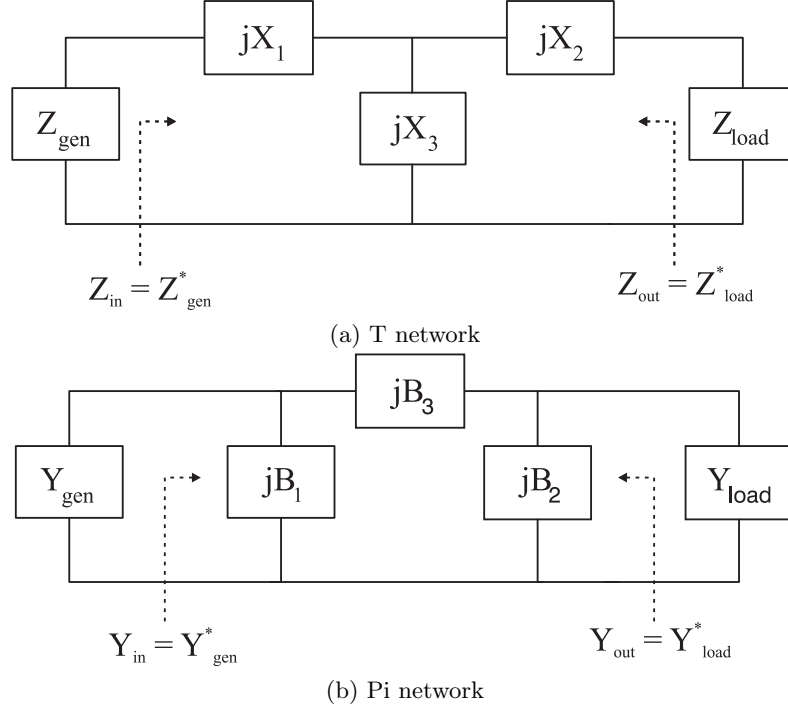


Figure 26: General lossless impedance and admittance matching network equivalent circuits

be either capacitors or inductors. These equivalent circuits naturally lend themselves to the design of lumped element matching networks and since the operating frequency of the radio assay is under 1 GHz, a lumped element matching network is practical. Therefore, the remainder of this section will focus on such a network, particularly the Pi network, shown in Figure 26b.

In order to achieve a conjugate match, illustrated in Figure 25, at both the load and generator, each pair of equations in (17) and (18) must be jointly satisfied.

$$\begin{aligned}
 \tilde{Z}_{gen}^* = \tilde{Z}_{gen} &= \frac{jX_3 (\tilde{Z}_{load} + jX_2)}{\tilde{Z}_{load} + j(X_2 + X_3)} + jX_1 \\
 \tilde{Z}_{load}^* = \tilde{Z}_{load} &= \frac{jX_3 (\tilde{Z}_{gen} + jX_1)}{\tilde{Z}_{gen} + j(X_1 + X_3)} + jX_2
 \end{aligned} \tag{17}$$

$$\begin{aligned}
 \tilde{Y}_{gen}^* = \tilde{Y}_{gen} &= \frac{jB_3 (\tilde{Y}_{load} + jB_2)}{\tilde{Y}_{load} + j(B_2 + B_3)} + jB_1 \\
 \tilde{Y}_{load}^* = \tilde{Y}_{load} &= \frac{jB_3 (\tilde{Y}_{gen} + jB_1)}{\tilde{Y}_{gen} + j(B_1 + B_3)} + jB_2
 \end{aligned} \tag{18}$$

Since there are two equations and three unknowns, each system is under constrained. Thus, the extra variable may be used to control network properties such as the phase shift and Q

of the circuit. If a conjugate match is only required at either the load or the generator, the problem reduces to that of an impedance transformer. In such a situation, the network satisfies the equations in (17) and (18) individually, not jointly.

3.2.3.3 Tunable Impedance Transformation Network Implementation

For the radio assay experiments presented in this report, a joint impedance match at the generator and load was not required. Therefore, an impedance transformation network was implemented to transform the load impedance into a match. For many applications, such an impedance transformation network must match a fixed load to a fixed generator impedance over a specified bandwidth. However, for the experiments presented in this report, the RF tag antenna impedance is not necessarily known and may vary depending upon the antenna being tested. The cause for this uncertainty lies in the manufacturing of the RF tag antennas as discussed in Section 3.2.1.4. As a result, the impedance transformation network must be tunable.

Sinsky and Westgate [28] and De Mingo et. al. [29], have both demonstrated such tunable networks. The transformation network presented in this report, is similar to that of Sinsky and Westgate [28]. The major difference is that Sinsky and Westgate use a computer algorithm to tune their network whereas the network for the radio assay is tuned manually. The tunable impedance transformation network was implemented using a Pi network as shown in Figure 27. The variable capacitors of the network were realized using BB833 varactor diodes from

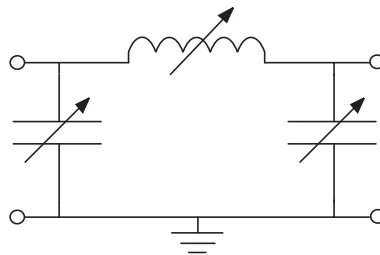


Figure 27: General tunable Pi impedance transformation circuit

Infineon. Varactor diodes provide a capacitance that is proportional to the applied, reverse-biased, DC voltage. Since variable inductors are difficult to construct, two J inverters were used to transform the capacitance of the varactor diode into an inductance, shown in Figure 28. The J inverter accomplishes this using the impedance inverting properties of a quarter wave

transmission line, shown in (19) and Figure 29.

$$\begin{aligned}
 Z_{in} &= \frac{Z_o^2}{\tilde{Z}_{cap}} \\
 &= j\omega C Z_o^2 \\
 &= j\omega L_{eq}
 \end{aligned}
 \tag{19}$$

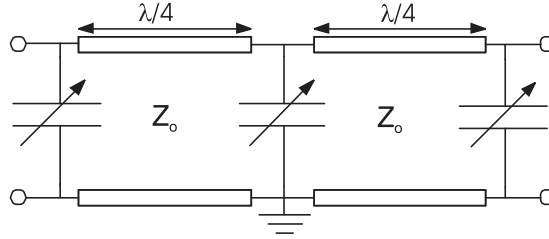


Figure 28: Tunable impedance transformation circuit using varactor diodes for capacitors and two J inverters to transform the center capacitance into an inductance

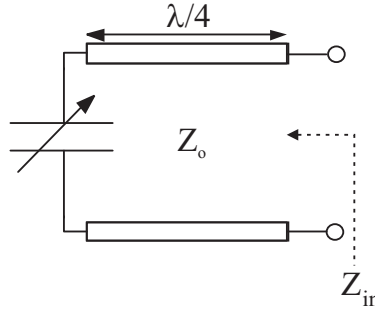


Figure 29: J inverter equivalent circuit

Since the varactor diodes are directly connected to the high frequency, RF signal, the DC bias voltages used to vary the capacitance must be separated from the RF portion of the network by a biasing network, shown in Figure 30a. The varactor diode is connected between the $50\ \Omega$ RF microstrip line and a $50\ \Omega$, open circuit, quarter wave line. The quarter wave line provides an equivalent short circuit, or virtual ground, to the RF signal that connects in series with the capacitance of the varactor diode. At this virtual ground, a DC bias voltage is applied to the cathode of the diode through an RF choke (CoilCraft 82nH chip inductor). The choke appears as a high impedance to the RF signal, but acts as a short circuit to the DC voltage. Thus, the DC bias voltage is supplied to the diodes while the DC and RF portions of the network remain separated. The DC return current passes through the RF signal line, through an RF choke, and

then is grounded at the DC ground via. The Pi impedance transformation network is realized

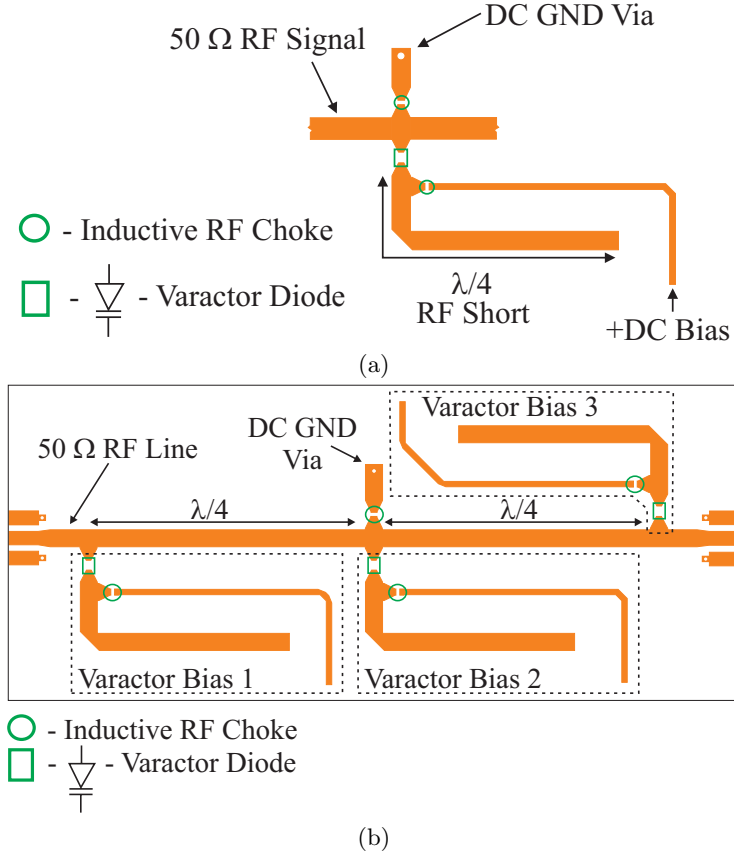
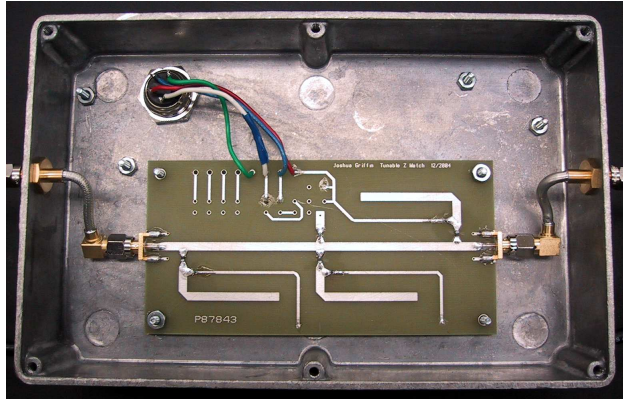


Figure 30: (a) Varactor diode bias network and (b) impedance transformation board layout

by simply connecting the three bias networks in series as shown in Figure 30b, and using the 50 Ω RF microstrip line as the common reference. Note, in Figure 30b, the center varactor diode is connected to the rest of the network via two quarter wave transmission lines, or J inverters. Therefore, as mentioned previously, the center varactor serves as a variable inductor. The tunable impedance transformation network is housed in a metal box for mechanical protection and RF shielding as shown in Figure 31.

The tunable impedance transformation network is tuned using three ten-turn potentiometers, illustrated in Figure 32. The bias voltage for the varactor diodes can be varied between 0.01 and 20.1 VDC providing each varactor diode an approximate range of 0.8 pF to slightly greater than 9.3 pF. Additionally, the approximate range of the variable inductor was 2 nH to slightly greater than 23.3 nH. The DC voltage was supplied by the regulated power supply illustrated in Figure 32a.

The tunable impedance transformation network is tuned by minimizing the return loss



(a)



(b)

Figure 31: (a) Tunable impedance transformation network board and (b) tunable impedance transformation network box with directional couplers at the input and output

measured at the input of the network, shown in Figure 33, using a 15 dB directional coupler (Minicircuits ZEDC-15-2B). An open circuit reference was established by measuring the coupled signal with the output of the directional coupler connected to an open circuit. This reference represented the return loss of the network with 100% of the power reflected. Each subsequent measurement was then referenced to this value as follows:

$$\text{R.L. (dB)} = \text{Open Circuit Reference (dBm)} - \text{Coupled Signal (dBm)} \quad (20)$$

The insertion loss of the tunable impedance match circuit was measured via a 15 dB directional coupler (Minicircuits ZEDC-15-2B) at the output of the network shown in Figure 33. It was necessary to measure the insertion loss each time the network was tuned since the transformation network acts as a filter. As the network is tuned by varying the values of the capacitors and inductors, the gain of the network at a particular frequency also changes. The

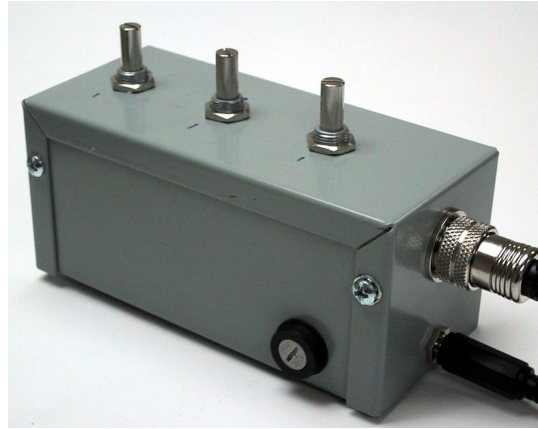
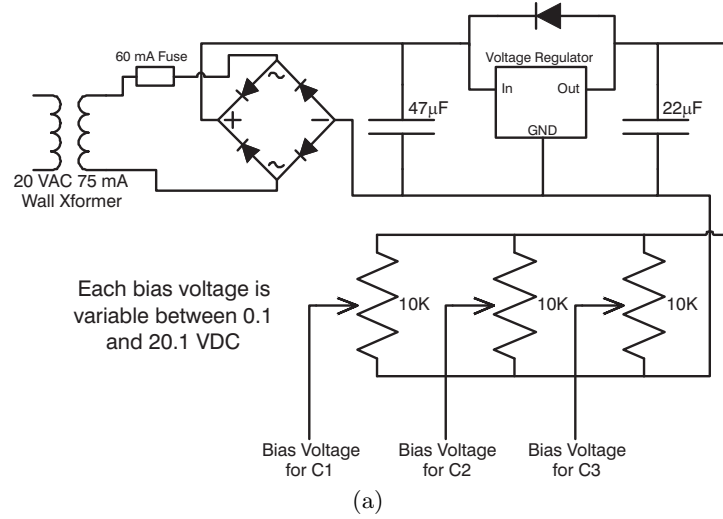


Figure 32: Tunable impedance transformation network control box (a) schematic and (b) photo

insertion loss was calculated as follows with a 15 dB factor to account for the 15 dB coupler:

$$\text{I.L. (dB)} = \text{Measured I.L. Signal (dBm)} - \text{Power Input to Network (dBm)} + 15 \text{ (dB)} \quad (21)$$

3.2.3.4 Justification of Feedback Method

As mentioned in Section 3.2.3.1, maximum power is transferred to the load when the equivalent input impedance is the complex conjugate of the generator impedance, $\tilde{Z}_{gen} = \tilde{Z}_{in}^*$ as shown Figure 20. In the radio assay experiments, the implemented impedance transformation network employs a directional coupler to provide feedback that is proportional to the power reflected from the load. To achieve a conjugate match, the impedance matching network is tuned to

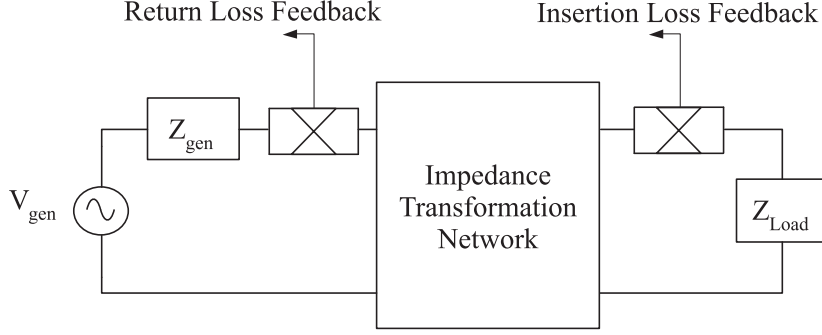


Figure 33: Tunable impedance transmission network with return loss and insertion loss direction couplers for feedback

minimize the return loss, or the reflected power from the equivalent input impedance, \tilde{Z}_{in} . By doing this, a true impedance match ($Z_{gen} = Z_{in}$) is achieved. The question arises as to whether or not this is equivalent to achieving a conjugate match. Pozar [27] addresses this issue and concludes that if the generator impedance is purely real, a true impedance match allows maximum power to be transferred to the load and is therefore, equivalent to a conjugate match. This result is shown by Pozar as follows [27]:

$$P_{avg-load} = \frac{1}{2} \left| \frac{\tilde{V}_{gen} \tilde{Z}_{in}}{\tilde{Z}_{in} + \tilde{Z}_{gen}} \right|^2 \operatorname{Re} \left\{ \frac{1}{\tilde{Z}_{in}} \right\} \quad (22)$$

Let $\tilde{Z}_{gen} = R_{gen} + jX_{gen}$ and $\tilde{Z}_{in} = R_{in} + jX_{in}$. If $\tilde{Z}_{gen} = \tilde{Z}_{in}^*$, then

$$R_{gen} = R_{in} \quad (23)$$

$$X_{gen} = -X_{in} \quad (24)$$

Substituting (23) and (24) into (16) gives the power transferred to the load if a conjugate match exists.

$$P_{avg-conjugate\ match} = \frac{1}{8} \frac{|\tilde{V}_{gen}|^2}{R_{gen}} \quad (25)$$

If a true impedance match is achieved, then ($Z_{gen} = Z_{in}$) and therefore, $R_{gen} = R_{in}$ and $X_{gen} = X_{in}$. Substituting these relationships into (16) gives the power transferred to the load.

$$\begin{aligned} P_{avg-true\ match} &= \frac{1}{2} \left| \frac{\tilde{V}_{gen} (R_{gen} + jX_{gen})}{2R_{gen} + j2X_{gen}} \right|^2 \operatorname{Re} \left\{ \frac{1}{R_{gen} + jX_{gen}} \right\} \\ &= \frac{1}{2} |\tilde{V}_{gen}|^2 \frac{1}{4} \frac{(R_{gen}^2 + X_{gen}^2)}{R_{gen}^2 + X_{gen}^2} \operatorname{Re} \left\{ \frac{R_{gen} - jX_{gen}}{R_{gen}^2 + X_{gen}^2} \right\} \\ &= \frac{1}{2} |\tilde{V}_{gen}|^2 \frac{1}{4} \frac{(R_{gen}^2 + X_{gen}^2)}{R_{gen}^2 + X_{gen}^2} \frac{R_{gen}}{R_{gen}^2 + X_{gen}^2} \end{aligned}$$

$$= \frac{1}{2} |\tilde{V}_{gen}|^2 \frac{1}{4} \frac{R_{gen}}{R_{gen}^2 + X_{gen}^2} \quad (26)$$

If \tilde{Z}_{gen} is real, then (26) reduces to (25). Consequently,

$$P_{avg-true\ match} = P_{avg-conjugate\ match} \quad (27)$$

Thus, when the return loss is minimized, maximum power is transferred to the load if the generator impedance is real. Since the signal source used in the radio assay has a purely real impedance of 50Ω , maximum power is indeed delivered to the load.

3.2.4 Directional Antennas

In order to conduct RF tag measurements, directional antennas are needed to focus EM energy on the tag antenna. Directional antennas provide the benefit of both focusing energy in a particular direction when transmitting and rejecting radiation that originates outside of its major lobe when receiving. Thus, a directional antenna is essential for accurate and repeatable measurements.

A horn antenna for 915 MHz, shown in Figure 34, was designed, constructed, and characterized by Yenpao “Albert” Lu. The horn has a 22 dB return loss when fed with a 50Ω coaxial line, a peak gain of 10.1 dBi, and a beamwidth of 40° .

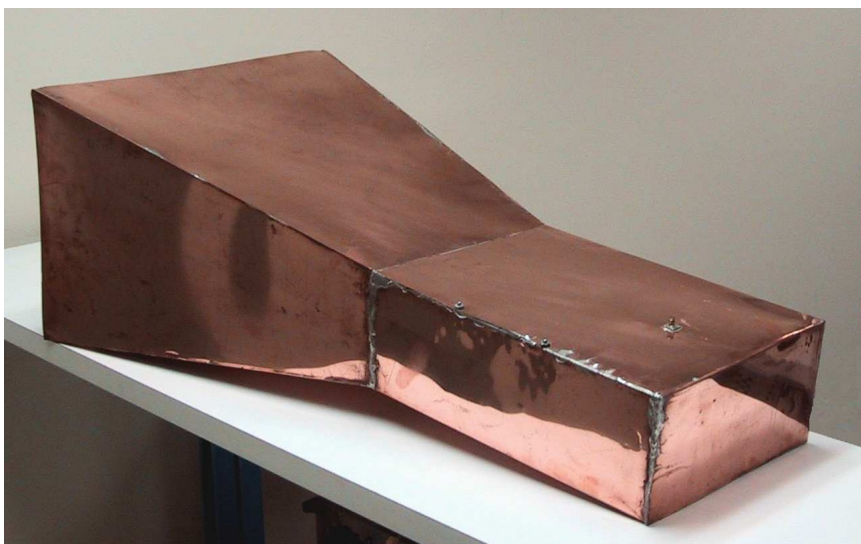
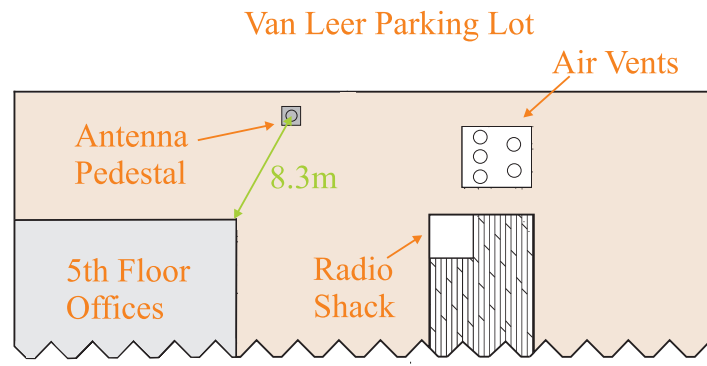


Figure 34: 915 MHz horn antenna with 40° beamwidth and 10.1 dBi peak gain.

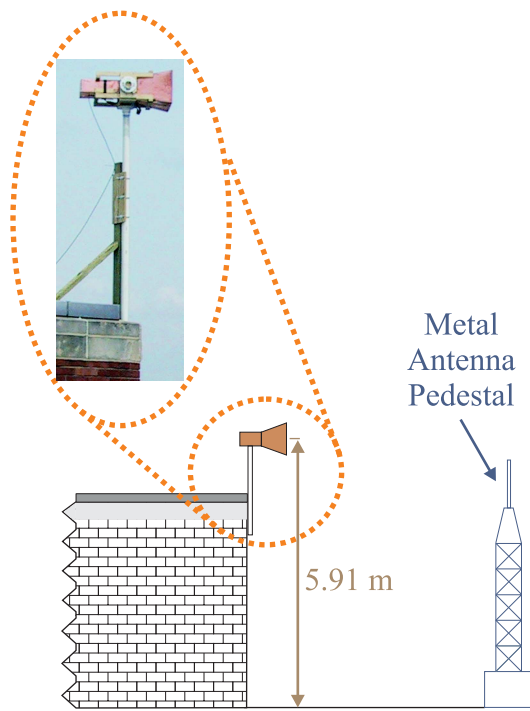
3.2.5 Antenna Range

For RF tag antenna experiments, it is important to conduct the experiments in a controlled environment. Typically, an antenna range is used for this purpose that is large enough for far field measurements and is free from scatterers. The antenna range used for the experiments presented in this report is located on the roof of the Van Leer Building as shown in Figure 35. The range consists of a stationary directional antenna and an antenna pedestal capable of rotating the antenna to be tested through 360° .

The stationary horn antenna, see Section 3.2.4, was mounted on the side of the 5th floor offices a distance of 8.3m from the antenna pedestal tower and a height of 5.91 meters above the roof. At 915 MHz, the horn antenna was 26λ away from the antenna pedestal tower allowing far field measurements to be taken. More information regarding modifications made to the antenna range for the radio assay experiments may be found in Section 4.3.



(a) Top view of outdoor antenna range located on the roof of the Van Leer Building



(b) Side view of the outdoor antenna range

Figure 35: Outdoor antenna range diagrams

CHAPTER IV

EXPERIMENTAL METHODS

This chapter discusses how the equipment described in Section 3.2 was implemented for the radio assay experiments presented in this report and the experimental methods used to conduct these experiments.

4.1 Radio Assay Equipment Setup

The radio assay experiments presented in this report used the following equipment:

- Agilent E4407B Spectrum Analyzer
- Agilent 8247C Continuous Wave Signal Generator
- Tunable Impedance Transformation Network (see Section 3.2.3.3)
- Balun and Transmission Line Topology Transformer (see Section 3.2.2)
- RF Tag Antennas (see Section 3.2.1)
- 915 MHz Horn Antenna (see Section 3.2.4)
- 1200 MHz Low Pass Filter and 900 MHz High Pass Filter
- RG58 Coaxial Cable

For both experiments, the equipment was set up as shown in Figure 36. The RF tag antenna was used to transmit a continuous wave (CW) signal at 915 MHz which was received by the horn antenna. The signal was filtered and measured by the spectrum analyzer which fed this data to a computer. The spectrum analyzer was set to a center frequency of 915 MHz with a resolution bandwidth of 10KHz. The CW signal generator output a +16 dBm signal for both the experiments.

Experimental Setup

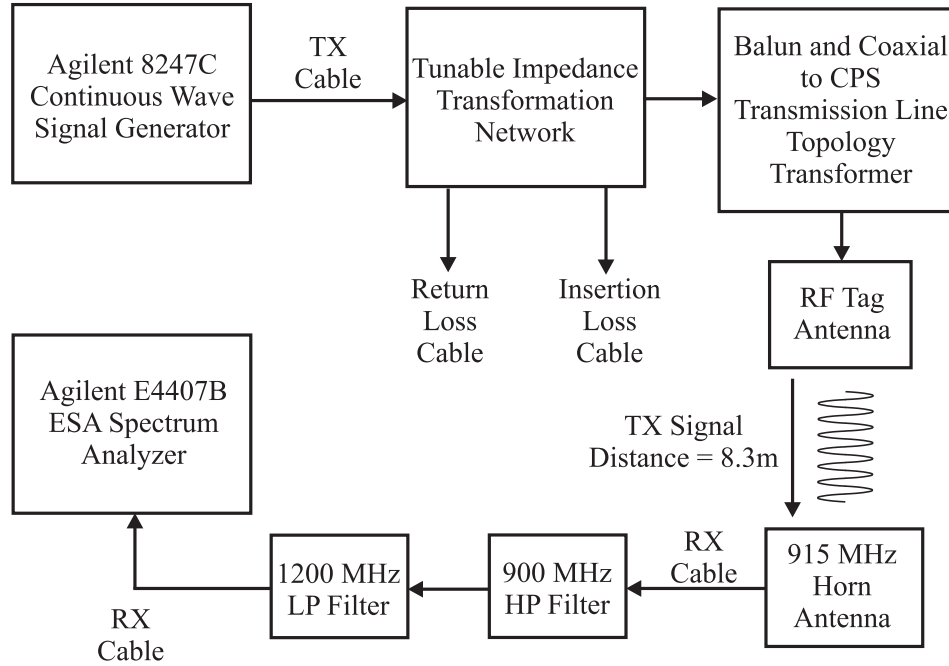


Figure 36: Diagram of radio assay experimental setup

4.2 RF Tag Antenna Feed and Attachment

Four RF tag antennas, as described in Section 3.2.1, were tested. Each antenna was fed using the quarter wave balun described in Section 3.2.2 and the coplanar strip (CPS) transmission line feed shown in Figure 37. Each RF tag antenna was connected to the CPS line using a clamp, shown in Figure 38a, to press the antenna against the two conducting strips of the CPS line feed. The clamp was made out of approximately 1/16 in. ($5/1000\lambda_o$) thick FR4 board with a permittivity $\epsilon \simeq 4.5$. This material was chosen instead of metal in order to minimize the clamp's effect on the fields surrounding the antenna. For this same reason, the clamp was held in place with nylon nuts and screws. The quarter wave balun, described in Section 3.2.2, connected to the CPS line was also designed to minimize its effect on the fields radiating from the antenna. This was accomplished by minimizing the size of the quarter wave balun and separating the RF tag antenna from the metal box housing the tunable impedance transformation network. Although the length of the quarter wave balun (approximately 41 cm or $1.25\lambda_o$) presented in this report was larger than the largest dimension of the RF tag antennas (16.5 cm or $\lambda_o/2$), the combined diameter of the coaxial feed line and the balancing line at the antenna feed was only

$0.03\lambda_o$. This diameter is not electromagnetically significant. Therefore, since the balun was fixed at a right angle to the antenna for the H plane measurements presented in this report, the length of the balun did not significantly affect the antenna performance. In other words, the balun was cross polarized with the RF tag antenna as shown in Figure 38a in Section 4.2. Since the balun length was not constrained (due to its orientation), the relatively long length of the balun was chosen to separate the RF tag antenna from the metal box housing the tunable impedance transformation network, discussed in Section 3.2.3.

The RF tag antenna was attached to each of the materials, described in Section 4.4 used in the radio assay experiments using thin adhesive tape. Holes were drilled into the solid materials to allow the antennas to lie as flat as possible along the material surface as shown in Figure 38b. The substrate of the CPS line was approximately $1/16$ in. ($5/1000\lambda_o$) thick and therefore, the flexible RF tag antennas were bent by that amount when attached to the materials. In the case of the baseline antenna, since it was made of rigid copper-clad FR4, it was not able to bend and was separated from the material by $1/16$ in. ($5/1000\lambda_o$). This distance is electromagnetically insignificant and the antennas were considered to lie flat against the material. When the antennas were attached to liquids, it was not possible for the CPS line substrate to lie flat on the surface due to the nuts holding the clamp as shown in Figure 39c. The distance of separation, b , was $1/4$ in. ($1/50\lambda_o$). Again, this distance is electromagnetically small and the antennas were considered to lie flat against the material.

4.3 Antenna Range Modifications

In the antenna range described in Section 3.2.5, the antenna pedestal tower was made of metal. If the RF tag antenna was directly attached to this structure, the measured antenna patterns would be significantly affected by the electromagnetically large metal structure. Therefore, an RF tag antenna mount was made in order to raise the RF tag antenna away from the metal pedestal tower. The RF tag antenna mount was constructed out of Polyvinyl Chloride (PVC) pipe and attached to the top of the antenna pedestal. PVC pipe was chosen for the mount because it has a low permittivity, low loss at 915 MHz, and high mechanical strength. The top of the antenna mount consists of a large, 19" x 18", rectangular structure to which the materials of the radio assay experiments were attached as shown in Figure 40. The antenna

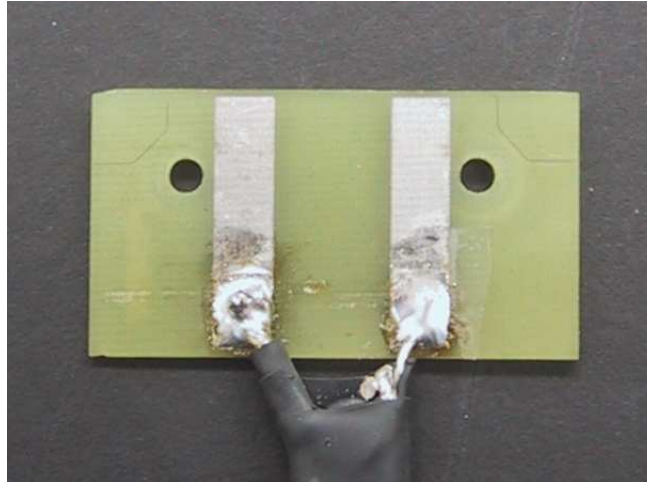
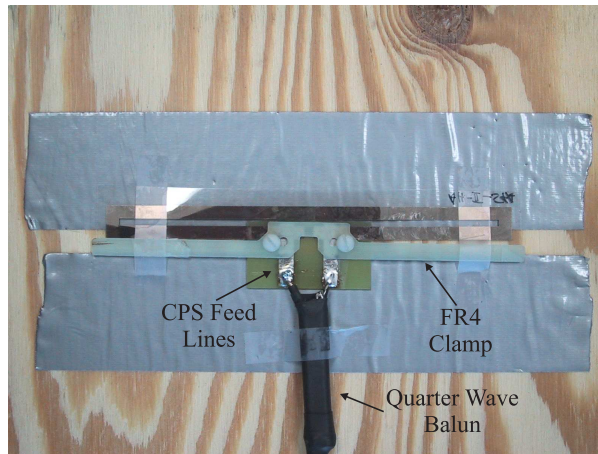
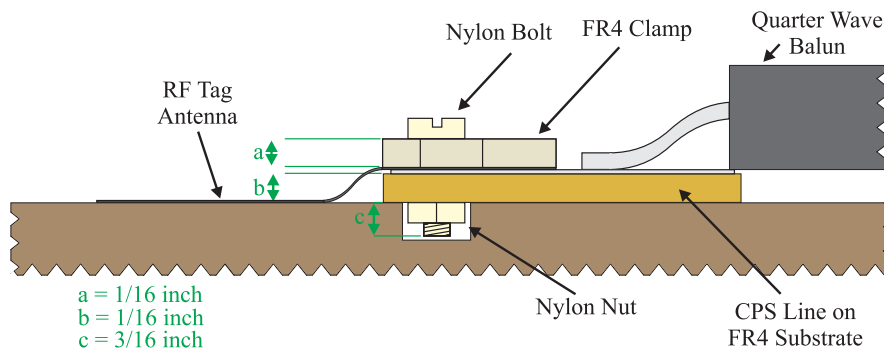


Figure 37: Quarter wave balun balanced terminals connected to the CPS transmission line antenna feed for the RF tag antennas



(a) RF tag antenna attached to solid material (wood)

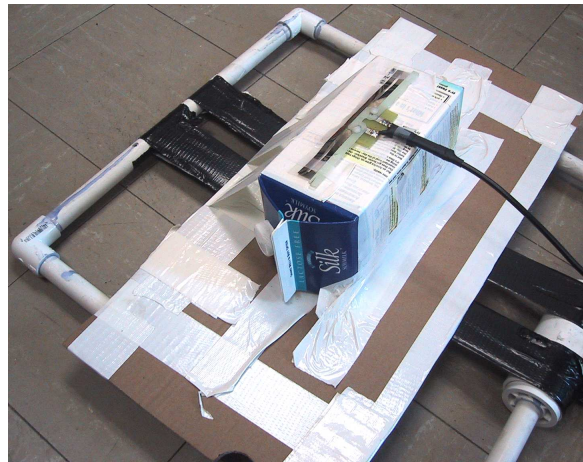


(b) Cross section of RF tag antenna and feed attached to solid material

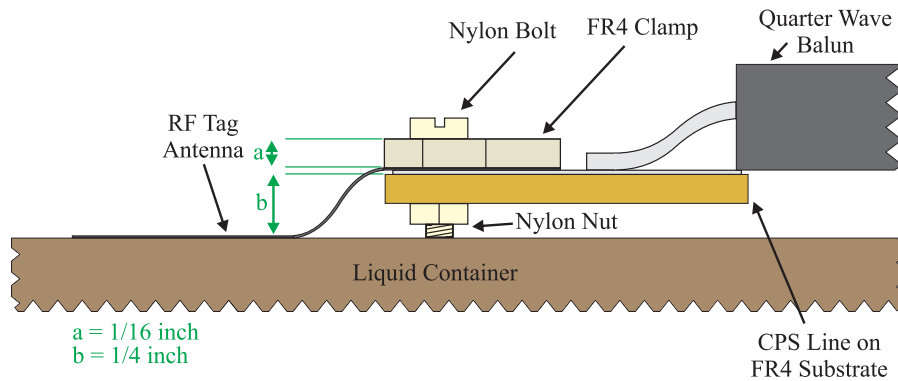
Figure 38: RF tag antenna attached to solid material



(a) Top view of the RF tag antenna attached to the liquid container



(b) Side view of the RF tag antenna attached to the liquid container



(c) Cross section of the RF tag antenna and feed attached to the liquid container

Figure 39: RF tag antenna attached to the liquid container

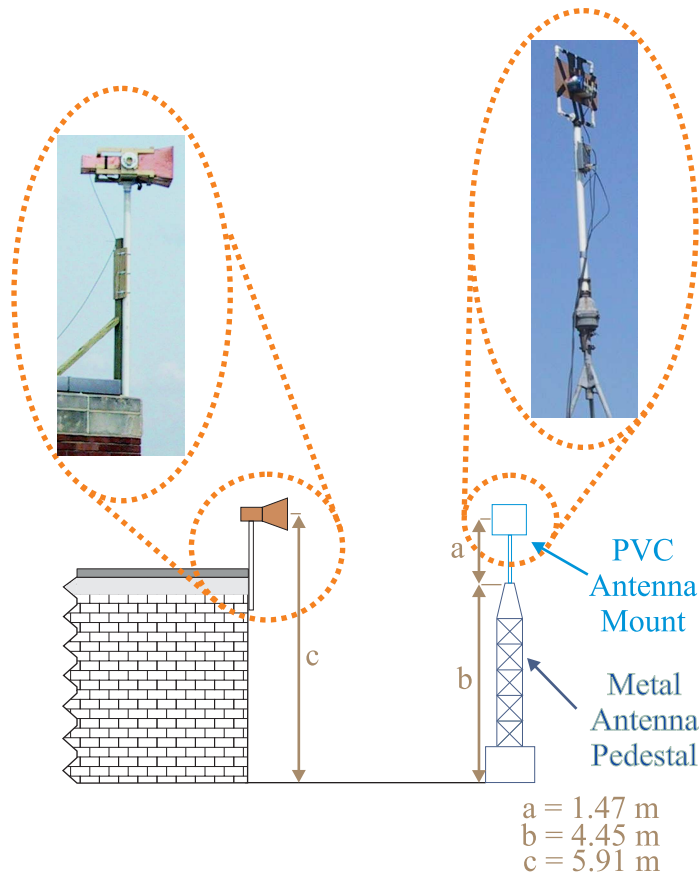


Figure 40: Side view of outdoor antenna range

mount raised RF tag antenna 1.47 m ($4.6\lambda_o$) above the metal antenna pedestal tower. Since the largest dimension of the RF tag antenna was 16cm, the antenna pedestal tower was in the far field of the RF tag antenna (Section 1.2.2.2), thus minimizing its effect on the antenna performance.

4.4 Radio Assay Materials

Seven materials, excluding free space, were used in the radio assay experiments presented in this report. These were cardboard, plywood, acrylic (plexiglass), distilled water, ground beef, automobile antifreeze (ethylene glycol), and aluminum. For simplicity, the remainder of this report will refer to these materials as cardboard, wood, acrylic, water, beef, ethylene glycol, and metal respectively. The goal in choosing these materials was to obtain materials that are in common use and that are candidates for having an RF tag attached. The listed materials meet this criteria and provide a variety of complex permittivities and conductivities. Table 6 presents the material properties of several materials as given by Von Hippel [30] at 300 MHz

	300 MHz		915 MHz		3 GHz		Radio Assay Equivalent
	ϵ	$\tan(\delta)$	ϵ^\dagger	$\tan(\delta)^\dagger$	ϵ	$\tan(\delta)$	
Plywood (Douglas Fir)	1.7	0.036	1.695	0.0357	1.5*	0.0220	Plywood (Pine)
Cardboard**	~ 1	~ 0	~ 1	~ 0	~ 1	~ 0	Cardboard (corrugated)
Plexiglass (Polymethyl Methacrylate)	2.66	0.0062	2.646	0.0061	2.6	0.0057	Plexiglass (acrylic)
Steak (bottom round)	50	0.7800	47.72	0.6707	40	0.3000	Ground Beef
Ethylene Glycol	39	0.1600	32.88	0.3513	12	1.0000	Anti-Freeze
Water	77.5	0.0160	77.32	0.0481	76.7	0.1570	Distilled Water

*Measured at 25 GHz

**Values for cardboard are not from Von Hippel, but were estimated to be that of air

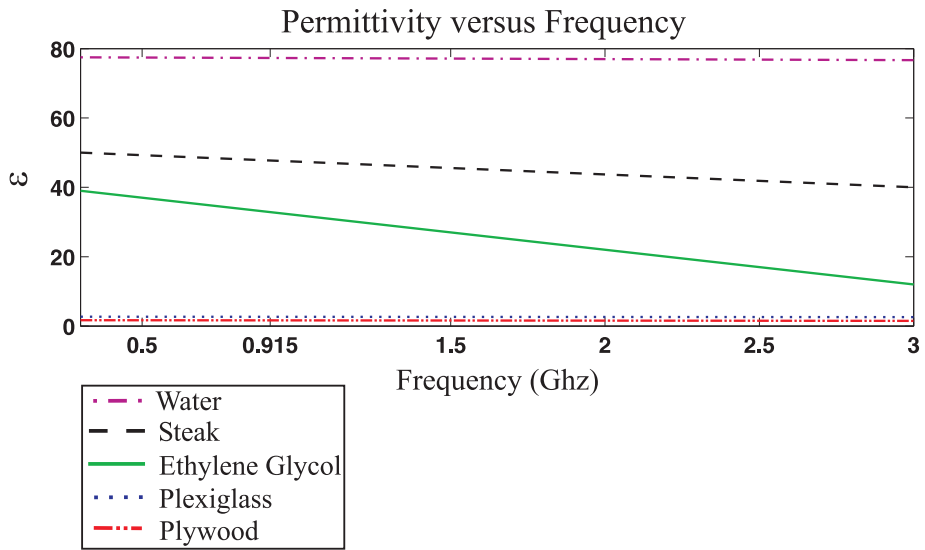
†These values were interpolated from the 300 MHz and 3 GHz data from Von Hippel

Table 6: Complex permittivity of materials for radio assay experiments

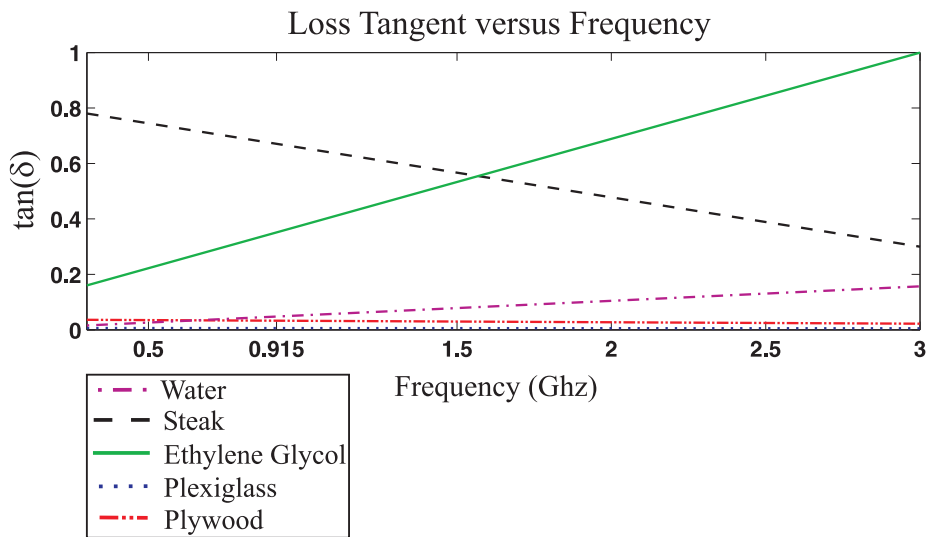
and 3 GHz. These values were used as estimates of the properties of the materials used in the radio assay experiments. The right most column of Table 6 displays the equivalent material used in the radio assay experiments. The permittivity and loss tangent values at 915 MHz were interpolated from the data given by Von Hippel. This data is illustrated graphically in Figure 41. A description of each of the materials and how each was prepared for the radio assay experiments is as follows:

Cardboard: Each sheet of cardboard was cut into a rectangle that was approximately 12 1/4" x 25 1/2" x 1/8". Several sheets were taped together to form 3 blocks that were each approximately 1/2" thick. Thus, each RF tag antenna was tested on 1 1/2" thick cardboard. Each of these three sheets was attached to the RF tag antenna mount using tape in a manner similar to that shown in Figure 42.

Wood: The wood used for the radio assay experiments was 3 layered plywood. Each piece of plywood was cut into a rectangle that was approximately 11 3/4" x 22 3/8" x 7/16". Three pieces of plywood were used to allow the antenna to be tested on 1.32" thick wood. The plywood was attached to the RF tag antenna mount using plastic zip ties as shown in Figure 42.



(a)



(b)

Figure 41: Interpolated (a) permittivity and (b) loss tangent values from Von Hippel [30]

Acrylic: Acrylic sheets, commonly known as plexiglass, were cut into pieces that were 6 1/8" x 24" x 7/32". Three blocks of acrylic, each 7/16" thick, were made by stacking the original acrylic pieces. The RF tag antennas were tested on the 1.32" thick acrylic block. Like the wood, the three acrylics sheets were attached to the RF tag antenna mount using plastic zip ties in a manner similar to that shown in Figure 42.

Metal: 22 gauge aluminum sheet metal was chosen for the metal of the radio assay experiments. Two metal sheets were bolted together to form a 18" x 22 3/4" sheet of aluminum that was attached to the RF tag antenna mount using plastic zip ties, in a manner similar to that shown in Figure 42. 22 gauge aluminum is approximately 0.025" thick.

Beef: The beef used in the radio assay was ground beef obtained from a local grocery store. At room temperature, the beef was formed into a rectangle that was approximately 4 1/2" x 9" x 1/2", placed in a thin sealable plastic bag, and taped to a thin piece of cardboard for support. The ground beef was suspended in the middle of the RF tag antenna mount using tape, shown in Figure 43.

Water: Distilled water was placed in a waxed cardboard carton for testing. The carton was attached to a 1/4" thick piece of cardboard and attached to the RF tag antenna mount using tape, shown in Figure 44. The dimensions of the carton were approximately 8 1/2" x 3 3/4" x 3 3/4". For testing, the carton was completely filled and the RF tag antenna taped to the center of the front side of the carton.

Ethylene Glycol: Commonly available anti-freeze was used for ethylene glycol in the radio assay. For the experiments, the anti-freeze was placed in the same container as the water and attached to the RF tag antenna mount in the same manner.

4.5 Radio Assay Calibration

The power received by an antenna is described by the Friis formula, which accounts for all of the antenna gains, path loss, and losses in the system.

$$P_R = P_t \frac{G_t G_d \lambda^2}{(4\pi r)^2 L_{\text{sys}}} \quad (28)$$



Figure 42: Electroless silver antenna attached to wood which is attached to the RF tag antenna mount

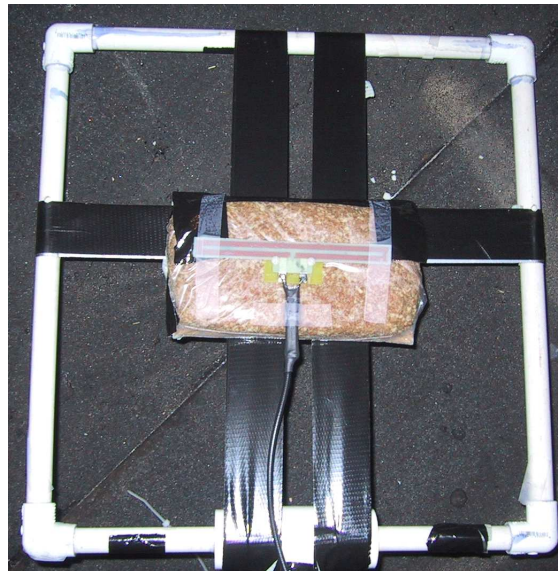


Figure 43: Baseline antenna on beef attached to the RF tag antenna mount

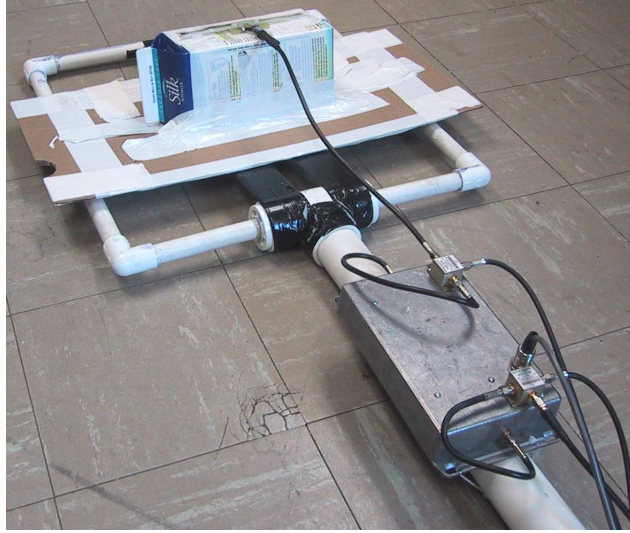


Figure 44: Electroless silver antenna attached to a milk carton on the RF tag antenna mount

or in decibel form

$$P_R = P_t - L_{\text{sys}} + G_t + G_r - 20\log_{10}\left(\frac{4\pi}{\lambda}\right) - 20\log_{10}(d) \quad (29)$$

where

P_R = Power received at the terminals of the receiving antenna

P_t = Power incident on the transmitting antenna

L_{sys} = System losses

G_t = Transmitter antenna gain

G_r = Receiver antenna gain

$20\log_{10}(d)$ = Free space path loss (referenced to 1m)

The Friis formula, in the form given above, assumes that each component in the system is well matched and that the antennas in the system are oriented for a polarization match. For the radio assay experiments, this assumption is valid. In order for the Friis formula to provide accurate results, each term must be identified and kept constant throughout the experiment. Typically, P_t , G_t , and the free space path loss are known or can be verified independently of the experimental setup. These parameters remain constant from measurement to measurement and need only to be verified once. The system losses, however, do not remain constant and

must be measured before each experiment. Possible sources of fluctuations in the system losses for the radio assay experiments were

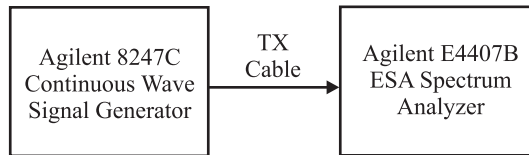
- Temperature changes
- Movement of scatterers in or near the antenna range
- Increasing cable losses due to bending and long term usage
- Connections that were not well seated

A back-to-back calibration procedure was followed to measure the losses in the system. When making loss measurements, the system included all possible cables, connectors, test instruments, and components that were present in the complete experimental setup. In addition, each time the system losses were measured, all of the test equipment was allowed to operate for at least 10-15 minutes to allow the equipment to reach a constant temperature. The goal of these steps was to measure the system losses with the system in the same state as it was for the experiments. To accomplish this, the experimental setup was connected as shown in Figure 45 and the losses in the receive cable, filters, insertion loss cable, return loss cable, and transmit cable were recorded at intervals throughout the radio assay experiments. The losses in the balun, tunable impedance transformation network, and the 915 MHz horn antenna could not be easily measured in the back-to-back calibration. The techniques used to measure these losses are discussed in each device's sections in Chapter 3.

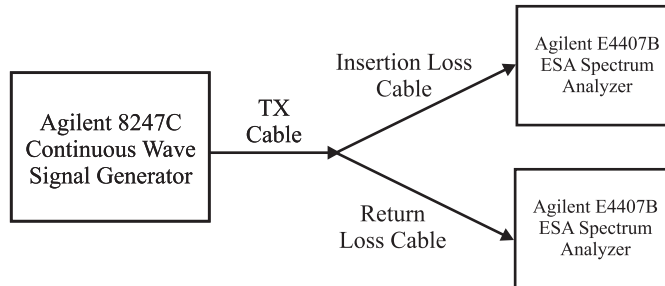
4.6 Calculations

All of the calculations presented in this report were based upon the Friis formula as presented in Section 4.5. When conducting the radio assay experiments, the following data was recorded:

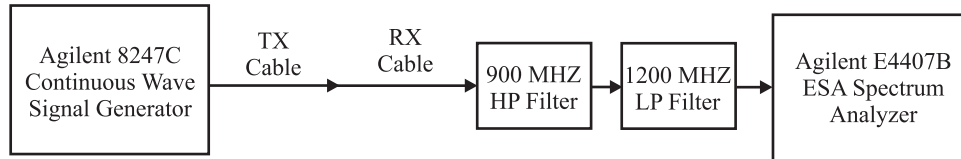
1. Losses in the transmit cable
2. Losses in the receive cable
3. Losses in the return loss cable
4. Losses in the insertion loss cable
5. Open circuit reference from the return loss directional coupler, see Section 3.2.3.3



(a) Equipment connections to measure loss in the transmit cable



(b) Equipment connections to measure loss in the insertion loss and return loss cables. Each loss measurement was performed separately



(c) Equipment to measure loss in the receive cable and filters

Figure 45: Equipment connections for the back-to-back calibration of the radio assay experimental setup

6. Return loss power - the power from coupled port of the return loss directional coupler when the antenna was tuned to both free space and the material
7. Power from the coupled port of the insertion loss directional coupler
8. Received power and the corresponding angles for pattern measurements

The calculations for the radio assay experiments were performed as follows:

Transformation network insertion loss (dB) =

$$\begin{aligned}
& P_{\text{Signal generator output (dBm)}} - P_{\text{TX cable loss (dB)}} \\
& - P_{\text{Recorded insertion loss measurement (dBm)}} \\
& + P_{\text{Insertion loss cable loss (dB)}}
\end{aligned} \tag{30}$$

$$\begin{aligned}
P_t \text{ (dBm)} &= P_{\text{Signal generator output (dBm)}} - P_{\text{TX cable loss (dB)}} \\
& - P_{\text{Transformation network loss (dB)}} - P_{\text{Balun loss (dB)}}
\end{aligned} \tag{31}$$

$$\begin{aligned}
P_r \text{ (dBm)} &= P_{\text{Recorded by the spectrum analyzer (dBm)}} + P_{\text{RX cable loss (dB)}} \\
& + P_{\text{Filter loss (dB)}}
\end{aligned} \tag{32}$$

$$\begin{aligned}
\text{Return Loss (dB)} &= P_{\text{O.C. return loss reference (dBm)}} \\
& - P_{\text{Recorded return loss measurement (dBm)}}
\end{aligned} \tag{33}$$

The gain of the RF tag antenna was found by inserting P_t and P_r into the Friis formula and solving (since the wave-length and distance are known). This yields:

$$G_t = P_r - P_t + L_{\text{sys}} - G_r + 20\log_{10}\left(\frac{4\pi}{\lambda}\right) + 20\log_{10}(d) \tag{34}$$

From this, the radiation efficiency of the antenna with respect to an ideal dipole may be found. The radiation efficiency is defined as

$$e_r = \frac{P_{\text{radiated}}}{P_t} \tag{35}$$

It accounts for losses in the antenna and is used to relate the gain and directivity of the antenna.

$$G = e_r D \tag{36}$$

If the antenna is 100% efficient ($e_r = 1$), the gain is equal to the directivity. Thus, the antenna gain with respect to an ideal dipole maybe calculated by dividing the measured antenna gain

by the ideal antenna directivity.

$$e_r = \frac{G}{D} \quad \text{or} \quad e_r = G \text{ (dBi)} - D \text{ (dBi)} \quad (37)$$

For the case of the ideal half wave-length dipole, the directivity is 1.64 or 2.15 (dBi).

4.7 RF Tag Antenna Orientation

For the radio assay experiments presented in this report, E-plane cuts of the antenna patterns were measured, as illustrated in Figure 46. For each measurement, the material was placed behind the antenna as shown in Figure 47. The region from -90° to $+90^\circ$ is the front region and the region from $+90^\circ$ to $+270^\circ$ is the back region as shown in Figure 47b.

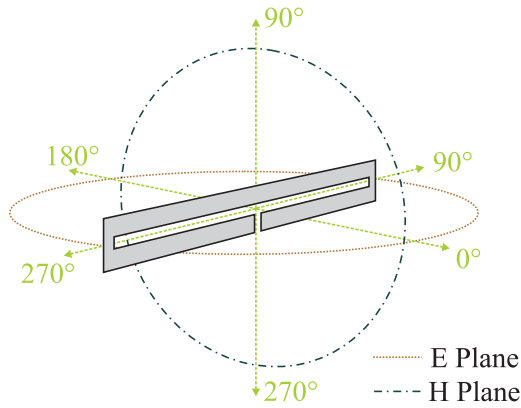
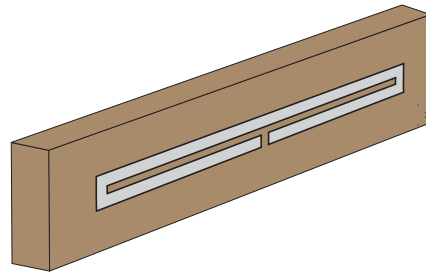
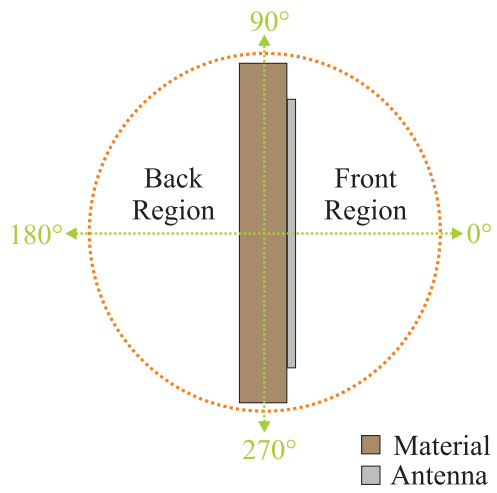


Figure 46: RF tag antenna E and H plane cuts



(a) Side view



(b) Top view

Figure 47: RF tag antenna orientation when attached to a material

CHAPTER V

RESULTS AND DISCUSSION

5.1 RF Tag Antenna Performance versus Antenna Material and Manufacturing Methods

The far field patterns of the four antennas described in Section 3.2.1, (i.e. Baseline, Silver, Copper, and ITO) were each measured in free space in order to compare the performance of the different antenna materials and antenna manufacturing methods. Figure 48 shows the measured far field antenna patterns. Note that these pattern measurements closely resemble those of an ideal dipole. The patterns contain no spurious lobes and are free from the effects of multi-path fading. In addition, there is no pattern distortion from cables or the metal antenna pedestal tower. This indicates that the outdoor antenna range, discussed in Section 3.2.5 and Section 4.3, is designed well. In addition, the baseline, silver, and copper antenna patterns have nulls at 90° and 270° that are greater than 25 dB down from the peak of the pattern. The ability to measure this shows that the balun is maintaining balanced currents at the RF tag antenna feed and not producing extraneous radiation. Table 7 summarizes the performance of the RF tag

Antennas in Free Space				
Tuned to Free Space	<i>Baseline</i>	<i>Silver</i>	<i>Copper</i>	<i>ITO</i>
Linearly Averaged Front Lobe Gain (dBi)	-4.9	-6.8	-7.2	-15.5
Linearly Averaged Front Lobe Efficiency (%)	19.6	12.8	11.6	1.7
Linearly Averaged Gain Penalty Relative to Baseline Antenna (dB)	0.0	1.8	2.3	10.6

Note: All calculations are based upon the front lobe (-90° to $+90^\circ$) values

Table 7: RF tag antenna performance characteristics in free space

antennas in terms of their front region (-90° to $+90^\circ$), linearly average values. For this report, the front region values were of interest since the RF tag antenna was attached to the front facing side of the materials, see Section 4.7.

Antenna patterns may contain several nulls, especially when they are attached to an object. Linearly averaging the values over the front region provides a way of characterizing the overall

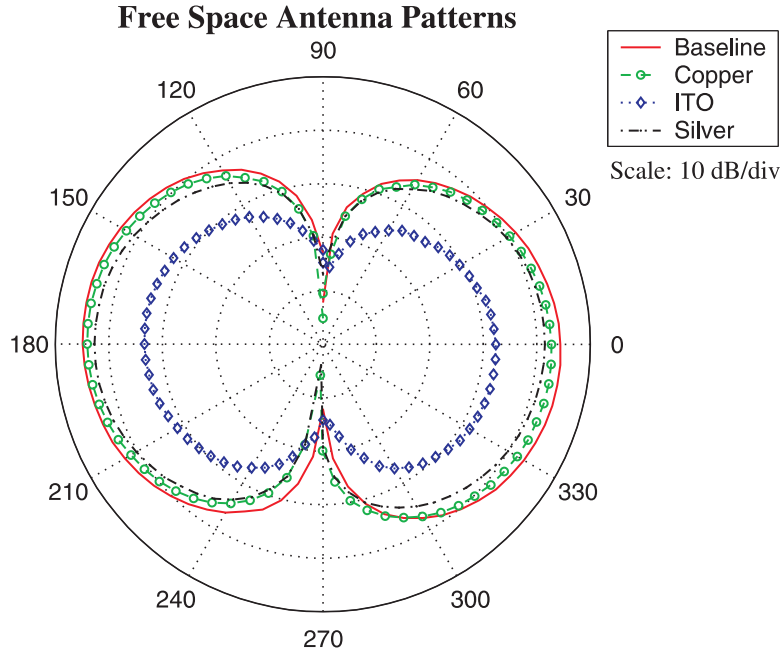


Figure 48: Far field pattern of RF tag antenna patterns in free space

front region antenna performance. The linearly averaged gain and radiation efficiency were calculated by setting $P_{R(\text{dBm})}$, in the Friis formula (Section 4.6), equal to the received power linearly averaged over the front region of the antenna pattern. To accomplish this, $P_{R(\text{dBm})}$ was converted into the linear scale, averaged from -90° to $+90^\circ$ and converted back into the logarithmic scale for calculations.

In this study, the linearly averaged gain relative to the baseline antenna is the most informative number presented. By studying the gains relative to the baseline antenna, any errors in the system (i.e. error the absolute gain of the receive antenna or error in the system losses) are subtracted out. Therefore, the gain relative to the baseline antenna provides the most accurate information to the RF designer concerning the antenna performance.

From Table 7, it can be seen that the baseline antenna has the best performance. This is expected since the baseline antenna has very low Ohmic losses and a conductor that is much thicker than the skin depth at 915 MHz ($\delta = 2.2 \mu\text{m}$). See Table 8.

The performance of the copper and silver antennas were roughly equal. Both antennas had higher Ohmic losses than the baseline antenna and the thickness of the conductors of both antennas were less than the skin depth at 915 MHz ($\delta_{\text{silver}} = 5.6 \mu\text{m}$, $\delta_{\text{copper}} = 6.4 \mu\text{m}$). Even so, the gains of these antennas were only approximately 2 dB less than that of the baseline

RF Tag Antennas					
	<i>Conductor Material</i>	<i>Antenna Substrate</i>	<i>Conductor Thickness</i>	<i>Bulk Conductivity</i>	<i>DC Resistance</i>
Baseline	1 oz. Copper	Rigid FR4	35.5 μm	5.7x10 ⁷ * S/m	0 Ω
Silver	Electroless Silver	Flexible PET**	202 \pm 19nm	8.9x10 ⁶ *** S/m	36 Ω
Copper	Electroless Copper	Flexible PET	195 \pm 17nm	6.8x10 ⁶ *** S/m	49 Ω
ITO	Indium Tin Oxide	Flexible PET	1 μm	1.6x10 ⁴ *** S/m	4K Ω

*Value from Stutzman and Thiele [12]

**PET - Polyethylene Terephthalate

***Estimated value calculated from the DC resistance and antenna geometry

Table 8: RF tag antenna physical characteristics reprinted from Table 3 in Section 3.2.1.4

antenna. The ITO antenna showed the poorest performance of the antennas tested with a -10 dB relative gain. Its Ohmic losses were considerably more than the other antennas and its thickness much was less than the skin depth at 915 MHz ($\delta_{\text{ITO}} = 131.5 \mu\text{m}$). Although the choice of an antenna for a particular design is dependent upon many factors, these results show that each of the tested antennas is a potential candidate for use in an RF tag.

5.2 RF Tag Antenna Performance versus Material Attachment

To study the RF tag antenna performance when attached to various materials, each RF tag antenna was attached to the seven materials discussed in Section 4.4 and the far field pattern of each antenna was measured. In this experiment, the tunable impedance transformer was tuned to the material upon which the RF tag antennas were attached. As stated in Section 3.1, the goal of this experiment was to determine the average decrease in antenna gain, or gain penalty, due to the material to which the tag antenna was attached. These values were calculated as shown in Figure 49. Table 9 displays the average antenna gain penalties for each material and these values are plotted in Figure 50. The far field antenna patterns and the complete tabulated data from these measurements are presented in Appendix A. From Figure 50 and Table 9 it can be seen that cardboard causes the least gain penalty while metal causes the highest. A comparison of Figure 50 and Figure 41 shows that the average antenna gain penalty increases with the increasing loss tangent of the material.

water, described by Figure 56, was unique in that it forms three distinct lobes centered at 0° in the front region. The changes in the antenna patterns on each material cannot be attributed to a single phenomenon. Surface waves in the material, diffraction around the material, the permittivity of the material, and the loss tangent of the material all contribute the shape of the pattern.

5.3 Antenna Performance versus Impedance Tuning

The goal of this experiment was to determine the RF tag antenna performance improvements that could be realized by tuning the impedance transformation network for an impedance match for each material to which the antenna was attached. For this experiment, each RF tag antenna material measurement was performed with two separate impedance matches.

Free Space Tuned Measurement Each RF tag antenna was placed on the RF tag antenna mount without a material attached. The tunable impedance transformation network was tuned for a low return loss. Each RF tag antenna was then attached to each material and measured *without* changing the tuning. The new return loss when attached to the material was recorded for each measurement.

Material Tuned Measurement Each RF tag antenna was attached to the material and the tunable impedance transformation network was tuned for a low return loss.

Table 10 shows a comparison of the RF tag antenna gain penalties for the antennas when tuned to free space and when tuned to the material. Figure 50 plots these average antenna gain penalties, calculated as shown in Figure 49, along with the data points used to calculate the average. From Figure 50, it is clear that the radio assay shows little difference between the tuning methods. The reason that the free space tuning and material tuning measurements are similar is clear when the return loss values are examined. Table 11 shows the range of the measured return losses of the free space tuned antennas when attached to various materials and the percentage of power lost due to the impedance mismatch. The average return loss values are plotted in Figure 51 along with the data points used to calculate the average. Even on metal, the material with the highest antenna gain penalty, the average return loss is greater than 10 dB and therefore, very little of the power is reflected. Since the average return loss

Range of RF Tag Antenna Gain Penalty Due to Material Losses				
	Material Tuned		Free Space Tuned	
	<i>Minimum (dB)</i>	<i>Maximum (dB)</i>	<i>Minimum (dB)</i>	<i>Maximum (dB)</i>
Cardboard	0.3	1.0	0.0	1.1
Acrylic	0.6	1.5	0.2	1.7
Wood	3.9	5.2	4.1	5.2
Ethylene Glycol	3.4	8.6	3.5	8.8
Water	5.5	6.4	5.5	6.6
Beef	5.1	13.6	5.1	13.4
Metal	5.9	12.0	5.5	12.0

Table 10: Range of the decrease in the linearly averaged RF tag antenna gain when the tunable impedance transformation network was tuned to the material and when it was tuned to freespace

values remain reasonably high when the free spaced tuned antennas are placed on the materials, the performance gains realized by tuning the antennas is quite small.

5.4 Guidelines for RF Tag Design

For the design of an RF tag system, careful planning of the wireless link power budget is required in order to ensure that the RF tags operate as desired. A basic link budget is given by the Friis formula discussed in Section 4.5 which accounts for factors such as the reader and tag antenna gains, the power transmitted from the reader antenna, the distance from the tag to the reader, the losses in the reader and RF tag systems, and the carrier frequency. This link budget works well for RF tag systems in which the tag operates in free space. However, nearly all RF tags are attached to objects whose properties degrade the performance of the tag antenna. To account for this, the basic link budget equation is modified as follows:

$$\begin{aligned}
 P_{\text{tag}} &= P_{\text{reader}} - L_{\text{sys}} + G_{\text{reader}} + G_{\text{tag ideal}} - \boxed{\text{Penalty}} \\
 &\quad - 20\log_{10}\left(\frac{4\pi}{\lambda}\right) - 20\log_{10}(d)
 \end{aligned}
 \tag{38}$$

where

$G_{\text{tag ideal}}$ = Gain of the RF tag antenna operating in an ideal environment

RF Tag Antenna Gain Penalty Due to Material Loss

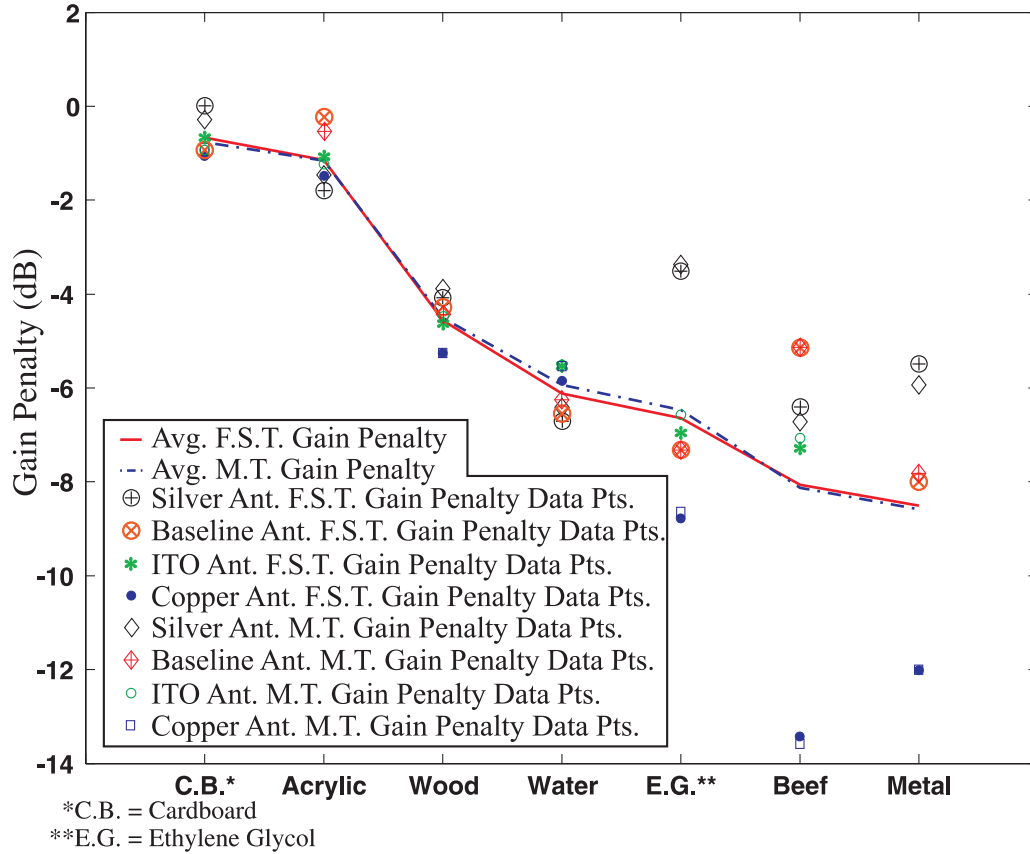


Figure 50: Free space and material tuned RF tag antenna gain penalties

P_{reader} = Power input to the reader antenna

L_{sys} = System losses in both the tag and reader systems

G_{reader} = Gain of the reader antenna

$20\log_{10}(d)$ = Free space path loss (referenced to 1 m)

Penalty = the RF tag antenna gain penalty due to (a) a lossy low cost RF tag antenna or (b) material loss

In this equation, it is assumed that the impedances are matched and that the antennas are oriented for a polarization match. Equation (38) is a one-way link budget template that allows the RF tag system design engineer to directly implement the results presented in this report. This template allows the designer to account for the diminished antenna performance of an RF tag antenna when it is attached to a material by substituting the average gain penalty values

Return Loss when Free Space Tuned Antennas are Applied to Materials				
	Return Loss		Percent Power Lost Due to Mismatch	
	<i>Minimum (dB)</i>	<i>Maximum (dB)</i>	<i>Minimum (%)</i>	<i>Maximum (%)</i>
Cardboard	31.9	34.6	0.03	0.06
Acrylic	8.6	16.4	2.3	13.8
Wood	10.6	16.7	2.1	8.7
Ethylene Glycol	13.8	15.9	2.6	4.2
Water	10.6	18.0	1.6	8.7
Beef	7.9	11.5	7.1	16.2
Metal	7.8	19.0	1.3	16.6

Table 11: Return loss and percentage of power lost due to the impedance mismatch of free space tuned antennas when attached to various materials

from Table 9 into $\boxed{\text{Penalty}}$ in equation (38). In addition, this template can account for the tag antenna performance reduction incurred when a low cost antenna is substituted for one of higher quality. For example, suppose a far field RF tag is designed to use a high quality, low loss folded dipole with a gain of 2 dB. If the RF design engineer wishes to replace this folded dipole with a low cost, electroless copper antenna, the designer simply substitutes the linearly averaged gain relative to the baseline antenna of the copper antenna from Table 7 into $\boxed{\text{Penalty}}$ in (38).

$$\begin{aligned}
 P_{\text{tag}} = & P_{\text{reader}} - L_{\text{sys}} + G_{\text{reader}} + \overbrace{G_{\text{tag ideal}}^{\text{=2 dB}}} - \overbrace{\boxed{\text{Penalty}}^{\text{=2.3 dB}}} \\
 & - 20\log_{10}\left(\frac{4\pi}{\lambda}\right) - 20\log_{10}(d)
 \end{aligned} \tag{39}$$

The effective tag antenna, $G_{\text{tag ideal}} - \boxed{\text{Penalty}}$, is equal to -0.3 dB. In order for the new RF tag with the copper antenna to receive the same amount of power as the original tag, the RF designer must do one of the following: increase the reader transmit antenna gain, increase the power to the reader transmit antenna, or decrease the RF tags distance from the reader. Now suppose this new RF tag with the copper antenna is placed upon a bottle filled with water.

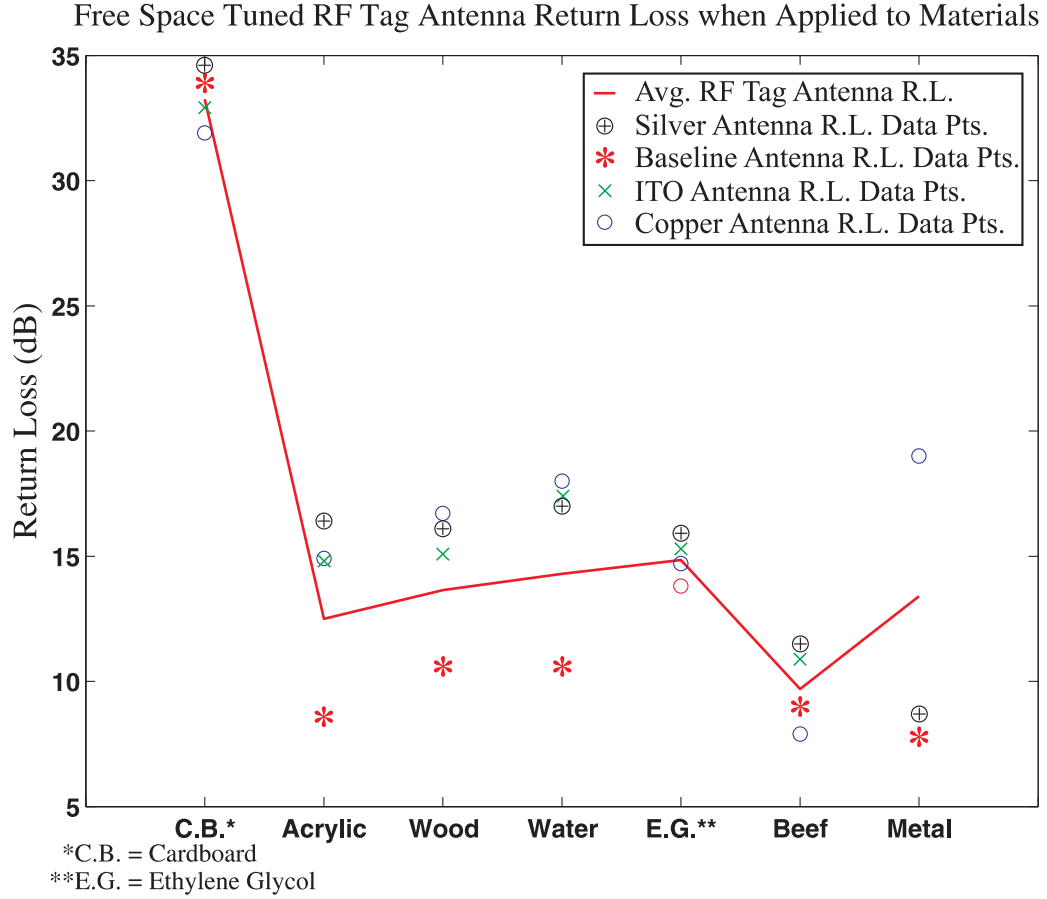


Figure 51: Return loss of free space tuned antennas when attached to various materials

From Table 10, the link budget is adjusted as follows:

$$\begin{aligned}
 P_{\text{tag}} &= P_{\text{reader}} - L_{\text{sys}} + G_{\text{reader}} + \overbrace{G_{\text{tag ideal}}^{\text{=2 dB}}}^{\text{=2.3+5.95}\pm\text{0.45 dB}} - \boxed{\text{Penalty}} \\
 &\quad - 20\log_{10}\left(\frac{4\pi}{\lambda}\right) - 20\log_{10}(d)
 \end{aligned} \tag{40}$$

The average gain penalty of water (5.95 ± 0.45 dB) has been added to the linearly averaged gain relative to the baseline antenna of the copper antenna (2.3 dB) in $\boxed{\text{Penalty}}$. The effective tag antenna gain is now equal to -6.5 ± 0.45 dB.

The one-way link budget determines the amount of power that can be transmitted to the RF tag for powering the tag memory and modulation circuitry. However, the communication of the far field tag via modulated backscatter requires a two-way link budget. A diagram of the two-way link is shown in Figure 52. In this setup, the reader antenna sends an RF signal to the tag. The RF tag receives this signal, modulates it, and reflects a portion of it back to the reader receive antenna. Note that in this system, the tag antenna gain acts on the reader

signal twice. The design formula template that governs the the two-way link is a modification of the radar equation defined by Stutman and Thiele [12].

$$\begin{aligned}
 P_{\text{reader-rx}} &= P_{\text{reader-tx}} - L_{\text{sys}} + G_{\text{reader-tx}} + G_{\text{reader-rx}} \\
 &+ 10\log_{10} \left(\frac{\sigma}{4\pi} \right) - 20\log_{10} \left(\frac{4\pi}{\lambda} \right) - 40\log_{10} (d)
 \end{aligned} \tag{41}$$

where

$G_{\text{reader-tx}}$ = Gain of the reader transmit antenna

$G_{\text{reader-rx}}$ = Gain of the reader receive antenna

P_t = Power input to the reader transmit antenna

$10\log_{10} \left(\frac{\sigma}{4\pi} \right)$ = Radar cross section of the RF tag antenna

L_{sys} = System losses in both the tag and reader systems

$40\log_{10} (d)$ = Free Space Path Loss for the two-way path(referenced to 1 m)

$20\log_{10} \left(\frac{4\pi}{\lambda} \right)$ = Frequency dependent loss

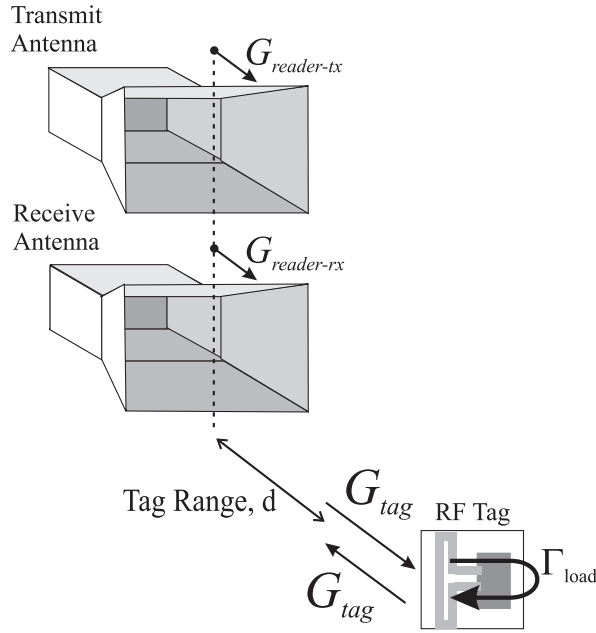


Figure 52: Diagram of an RF tag system far field backscatter communication link between a reader's transmit and receive antennas and an RF tag

The amount of backscattered radiation from an RF tag is determined by the radar cross section, σ , of the RF tag antenna. This cross section has two components, the antenna mode and the residual mode [12]. The antenna mode component is defined as follows:

$$\sigma_{\text{ant}} = \frac{(\Gamma_{\text{load}} G_{\text{tag}} \lambda)^2}{4\pi} \quad (42)$$

This component scatters radiation according to the antenna's pattern and is dependent upon the RF tag antenna gain, G_{tag} , the antenna load reflection coefficient, Γ_{load} , and the carrier frequency. The residual cross section component is not dependent upon the antenna radiation parameters or the load presented to the antenna. When the RF tag uses load modulation to encode the carrier signal, Γ_{load} is varied which, in turn, changes the antenna's antenna mode cross section. However, the residual mode cross section component does not vary with the load modulation, but remains constant (assuming the orientation of the tag and the reader do not change). Since an RF reader senses only the modulated backscatter, the residual cross section component is neglected in the two-way link budget template. By substituting σ_{ant} into (41), the following two-way link budget template was obtained:

$$\begin{aligned} P_{\text{reader-rx}} &= P_{\text{reader-tx}} - L_{\text{sys}} + G_{\text{reader-tx}} + G_{\text{reader-rx}} \\ &+ 20\log_{10}(\Gamma_{\text{load}}) + 2G_{\text{tag ideal}} - 2\boxed{\text{Penalty}} \\ &- 40\log_{10}\left(\frac{4\pi}{\lambda}\right) - 40\log_{10}(d) \end{aligned} \quad (43)$$

This template is to be used in the same manner as the one-way link budget template. Note that the tag gain in the two-way link budget is increased by a power of two (in the linear scale). Therefore, the gain penalties due to material losses and lossy antennas are also greater by a power of two.

CHAPTER VI

CONCLUSION AND SUGGESTED FUTURE WORK

6.1 Conclusion

To summarize, this report has provided an overview of basic RF tags and discussed the goals of current RF tag research - to reduce the tag cost, to decrease the tag footprint, and to improve the tag performance. To this end, this report has presented a radio assay for the study of RF tag antenna performance and results from several radio assay experiments. The results of the first experiment are measurements of the decrease in RF tag antenna gain as a function of the antenna material and manufacturing method. These results are compared to a baseline RF tag antenna and presented as a gain penalty in Section 5.1. Although many factors influence the choice of an antenna for a particular design, these measurements show that each antenna tested is a potential candidate for use in an RF tag. The results of the second experiment are measurements of the decrease in RF tag antenna gain when the antenna is attached to materials of varying electromagnetic properties. These results are compared to the free space gain of the antenna and are presented as gain penalties in Section 5.2. These results show that the antenna gain penalty due to material loss increases with the increasing loss tangent of the material. The third experiment shows the benefit of tuning the tag antenna for an impedance match when it is attached to a material over using the free space impedance match tuning. These results are discussed in Section 5.3. These results show that little benefit is derived from such tuning. Finally, the results from each of these experiments have been presented in a form that allows the RF tag system designer to directly apply them to an RF tag system link budget.

6.2 Suggested Future Work

The following radio assay experiments should be conducted in the near future to add value to the results that have been presented in this report.

- Perform the radio assay material measurement experiments described in Section 3.1 and Section 5.2 an expanded set of materials whose electromagnetic properties have been

measured.

- Measure the RF tag antenna performance as a function of antenna deformation
- Measure the RF tag antenna performance as a function of the reader polarization match

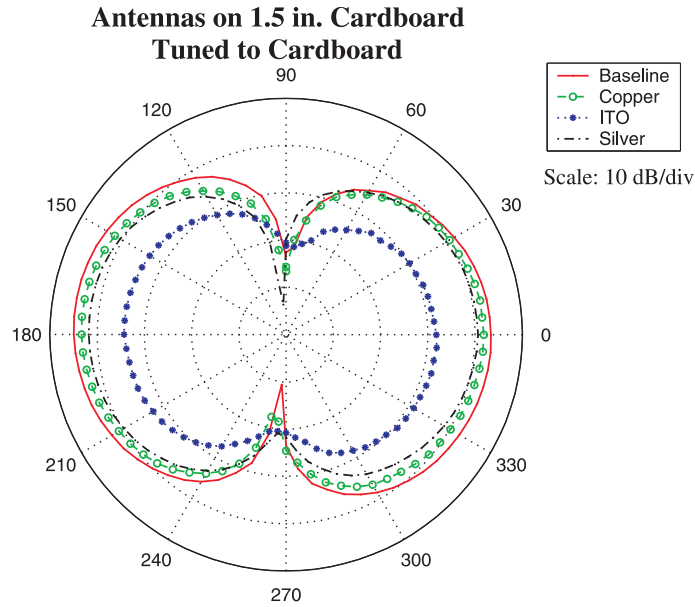
Several other experiments are possible with modifications to the radio assay experimental setup as discussed in Section 3.1. It is recommended that these experiments also be conducted. These experiments include:

- RF tag antenna performance in the presence of nearby objects with various electromagnetic properties
- Optimal RF tag reader antenna topologies
- RF tag antenna diversity experiments
- Characterization of small-scale fading in RF tag systems

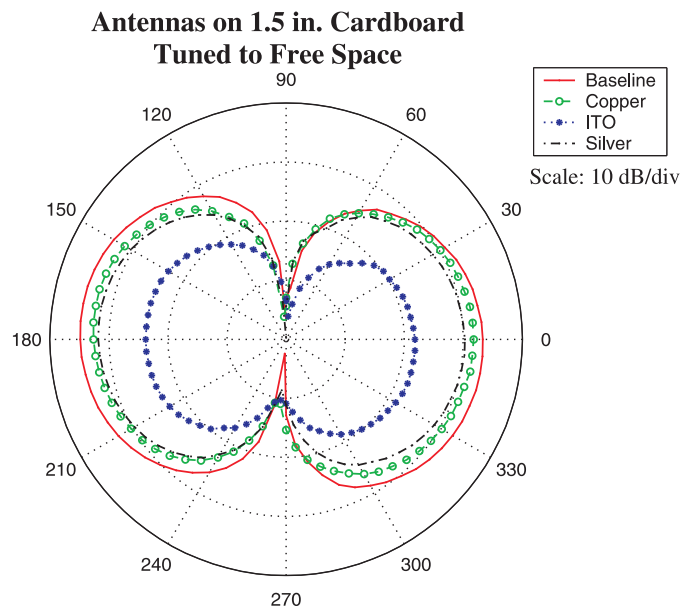
APPENDIX A

TABULATED DATA FROM THE RF TAG ANTENNA

MATERIAL MEASUREMENTS



(a) Tuned to Cardboard



(b) Tuned to Free Space

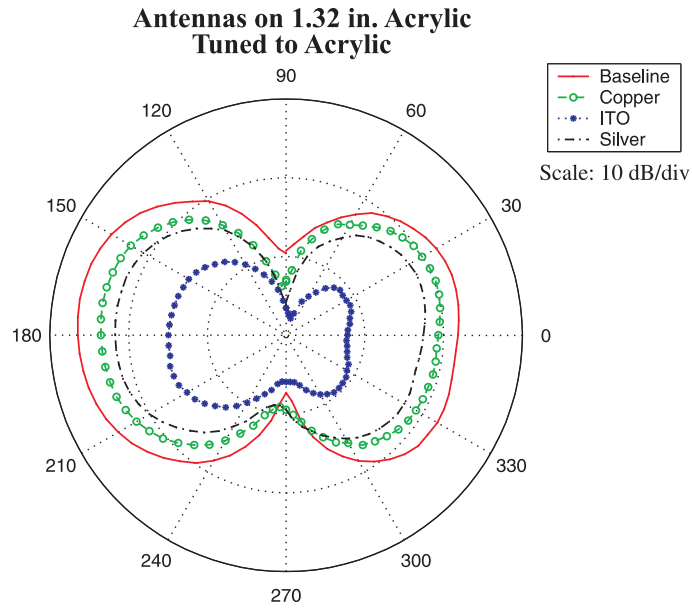
Figure 53: Four RF tag antennas attached to 1.5 inch thick Cardboard

Four RF Tag Antennas on 1.5 inch thick Cardboard				
Tuned to Cardboard	<i>Baseline</i>	<i>Copper</i>	<i>ITO</i>	<i>Silver</i>
Linearly Averaged Front Lobe Absolute Gain (dB)	-5.9	-8.2	-15.8	-7.7
Linearly Averaged Front Lobe Efficiency (%)	15.7	9.3	1.6	10.5
Linearly Averaged Gain Penalty Relative to Free Space Gain (dB)	1.0	1.0	0.3	0.9
Tuned to Free Space				
Linearly Averaged Front Lobe Absolute Gain (dB)	-5.9	-7.9	-15.5	-7.8
Linearly Averaged Front Lobe Efficiency (%)	15.8	9.9	1.7	10.0
Linearly Averaged Gain Penalty Relative to Free Space Gain (dB)	0.9	0.7	0.0	1.1

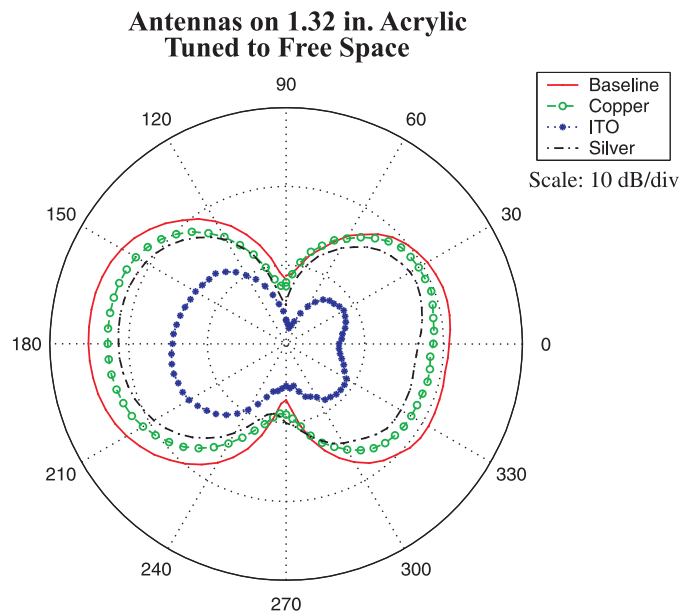
Table 12: RF tag antenna performance characteristics when attached to 1.5 inch thick cardboard

Four RF Tag Antennas on 1.32 inch thick Acrylic				
Tuned to Acrylic	<i>Baseline</i>	<i>Copper</i>	<i>ITO</i>	<i>Silver</i>
Linearly Averaged Front Lobe Absolute Gain (dB)	-5.5	-8.3	-17.0	-8.2
Linearly Averaged Front Lobe Efficiency (%)	17.2	9.0	1.2	9.1
Linearly Averaged Gain Penalty Relative to Free Space Gain (dB)	0.6	1.1	1.5	1.5
Tuned to Free Space				
Linearly Averaged Front Lobe Absolute Gain (dB)	-5.2	-8.3	-17.3	-8.3
Linearly Averaged Front Lobe Efficiency (%)	18.6	9.0	1.1	9.1
Linearly Averaged Gain Penalty Relative to Free Space Gain (dB)	0.2	1.1	1.7	1.5

Table 13: RF tag antenna performance characteristics when attached to 1.32 inch thick acrylic

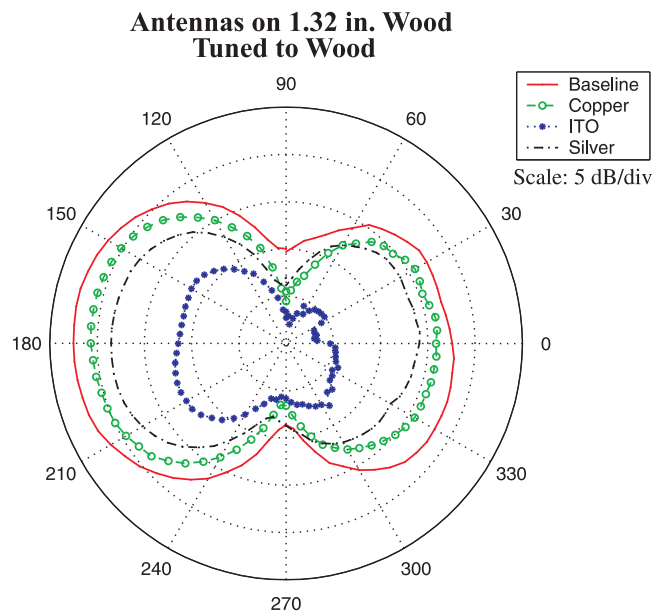


(a) Tuned to Acrylic

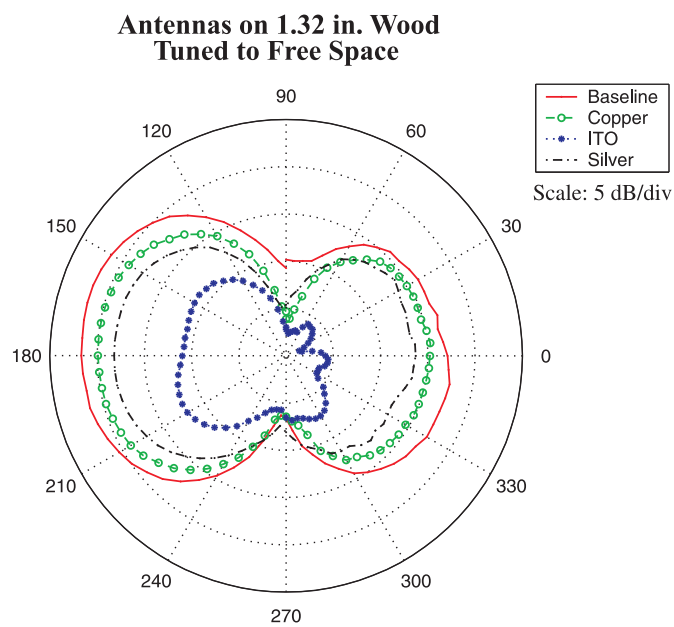


(b) Tuned to Free Space

Figure 54: Four RF tag antennas attached to 1.32 inch thick acrylic

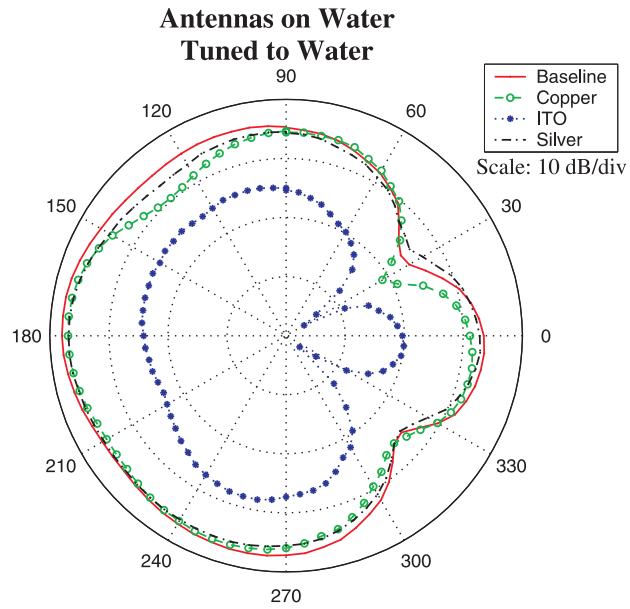


(a) Tuned to Wood

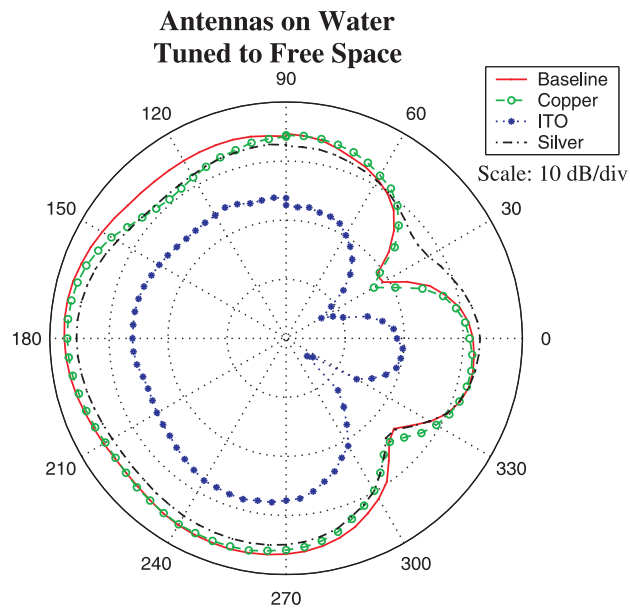


(b) Tuned to Free Space

Figure 55: Four RF tag antennas attached to 1.32 inch thick wood



(a) Tuned to Water



(b) Tuned to Free Space

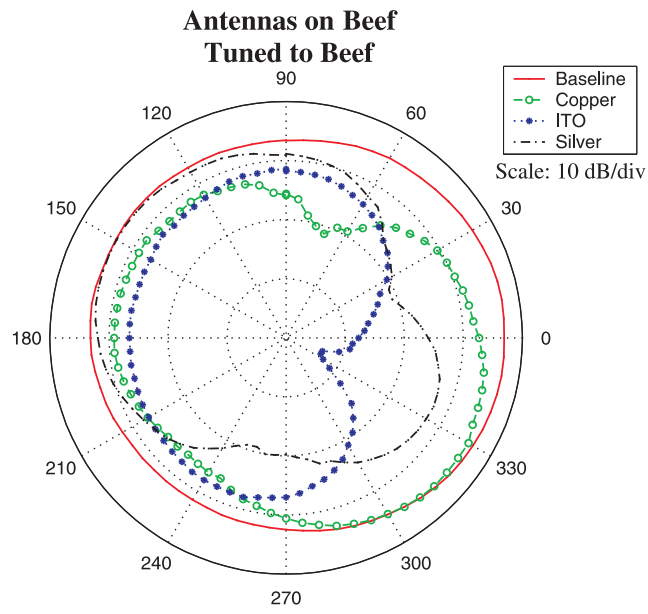
Figure 56: Four RF tag antennas attached to cardboard carton filled with water

Four RF Tag Antennas on 1.32 inch thick Wood				
Tuned to Wood	<i>Baseline</i>	<i>Copper</i>	<i>ITO</i>	<i>Silver</i>
Linearly Averaged Front Lobe Absolute Gain (dB)	-9.4	-11.7	-19.4	-12.0
Linearly Averaged Front Lobe Efficiency (%)	7.1	4.1	0.7	3.8
Linearly Averaged Gain Penalty Relative to Free Space Gain (dB)	4.4	4.5	3.9	5.2
Tuned to Free Space				
Linearly Averaged Front Lobe Absolute Gain (dB)	-9.2	-11.8	-19.6	-12.0
Linearly Averaged Front Lobe Efficiency (%)	7.3	4.0	0.7	3.8
Linearly Averaged Gain Penalty Relative to Free Space Gain (dB)	4.3	4.6	4.1	5.2

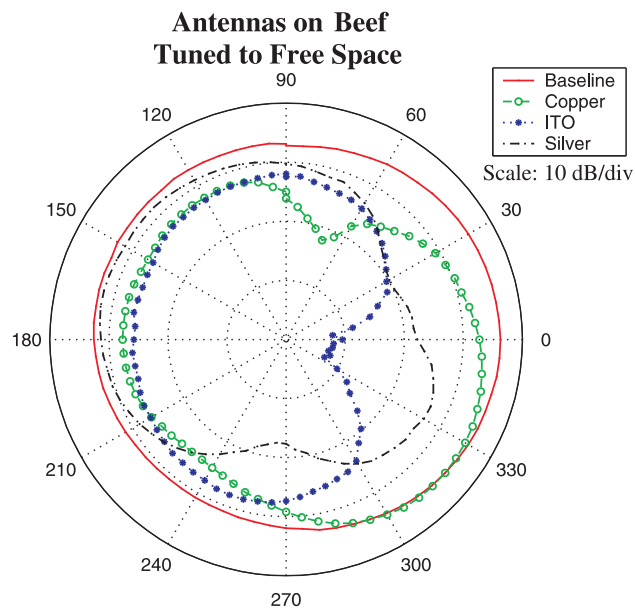
Table 14: RF tag antenna performance characteristics when attached to 1.32 inch thick wood

Four RF Tag Antennas on Water				
Tuned to Water	<i>Baseline</i>	<i>Copper</i>	<i>ITO</i>	<i>Silver</i>
Linearly Averaged Front Lobe Absolute Gain (dB)	-11.2	-12.7	-21.9	-12.3
Linearly Averaged Front Lobe Efficiency (%)	4.6	3.3	0.4	3.6
Linearly Averaged Gain Penalty Relative to Free Space Gain (dB)	6.3	5.5	6.4	5.5
Tuned to Free Space				
Linearly Averaged Front Lobe Absolute Gain (dB)	-11.5	-12.7	-22.1	-12.6
Linearly Averaged Front Lobe Efficiency (%)	4.4	3.2	0.4	3.3
Linearly Averaged Gain Penalty Relative to Free Space Gain (dB)	6.5	5.5	6.6	5.8

Table 15: RF tag antenna performance characteristics when attached to a cardboard carton filled with water

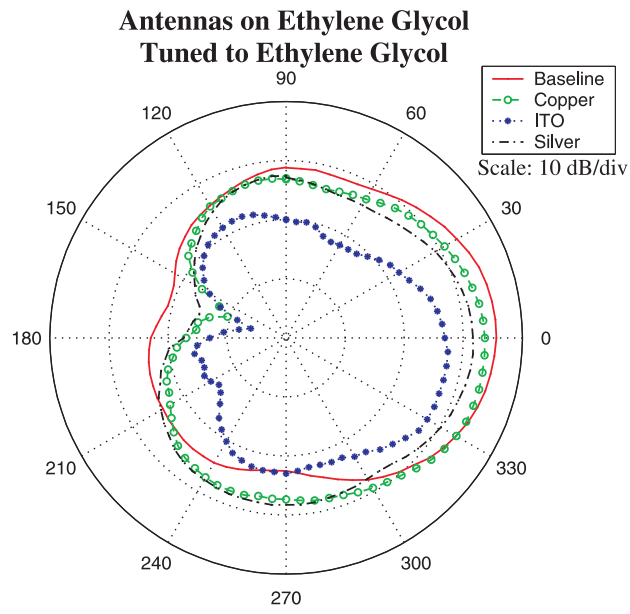


(a) Tuned to Beef

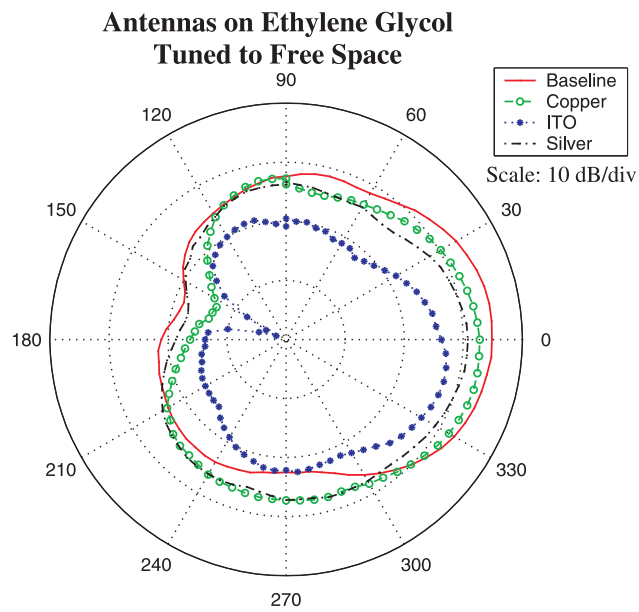


(b) Tuned to Free Space

Figure 57: Four RF tag antennas attached to beef enclosed in a plastic bag



(a) Tuned to Ethylene Glycol



(b) Tuned to Free Space

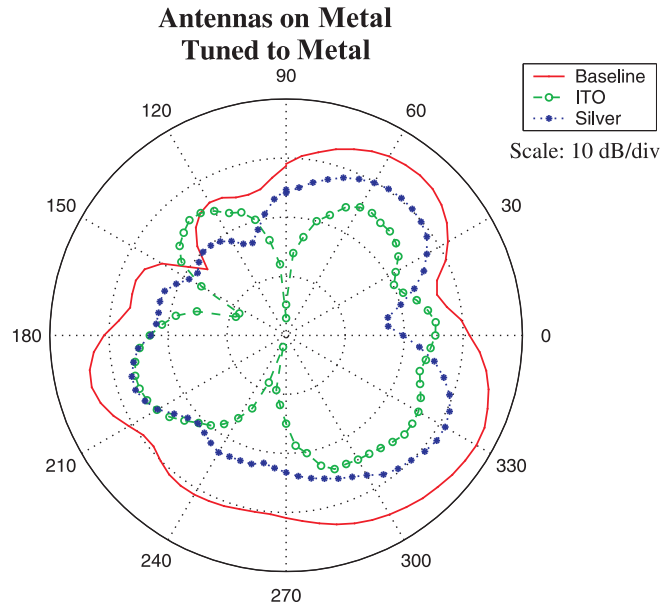
Figure 58: Four RF tag antennas attached to a cardboard carton filled with ethylene glycol

Four RF Tag Antennas on Beef				
Tuned to Beef	<i>Baseline</i>	<i>Copper</i>	<i>ITO</i>	<i>Silver</i>
Linearly Averaged Front Lobe Absolute Gain (dB)	-10.1	-14.3	-22.2	-20.3
Linearly Averaged Front Lobe Efficiency (%)	6.0	2.3	0.4	0.6
Linearly Averaged Gain Penalty Relative to Free Space Gain (dB)	5.1	7.1	6.7	13.6
Tuned to Free Space				
Linearly Averaged Front Lobe Absolute Gain (dB)	-10.1	-14.5	-21.9	-20.2
Linearly Averaged Front Lobe Efficiency (%)	6.0	2.2	0.4	0.6
Linearly Averaged Gain Penalty Relative to Free Space Gain (dB)	5.1	7.3	6.4	13.4

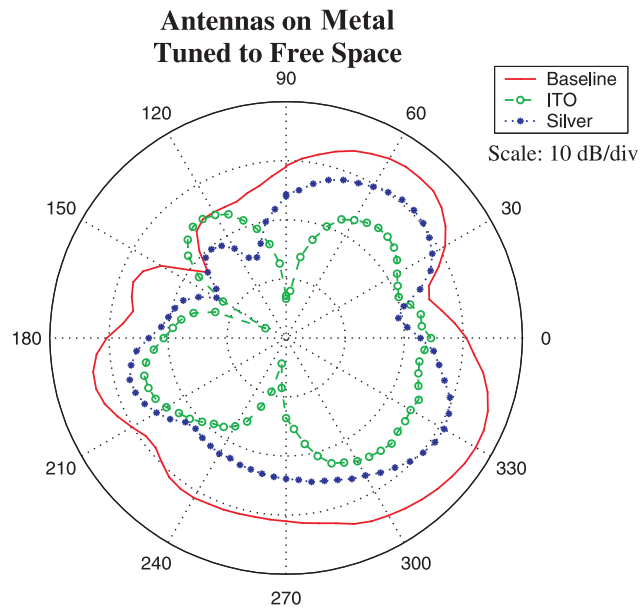
Table 16: RF tag antenna performance characteristics when attached to beef enclosed in a plastic bag

Four RF Tag Antennas on Ethylene Glycol				
Tuned to Ethylene Glycol	<i>Baseline</i>	<i>Copper</i>	<i>ITO</i>	<i>Silver</i>
Linearly Averaged Front Lobe Absolute Gain (dB)	-12.2	-13.8	-18.9	-15.4
Linearly Averaged Front Lobe Efficiency (%)	3.6	2.6	0.8	1.8
Linearly Averaged Gain Penalty Relative to Free Space Gain (dB)	7.3	6.6	3.4	8.6
Tuned to Free Space				
Linearly Averaged Front Lobe Absolute Gain (dB)	-12.2	-14.2	-19.0	-15.6
Linearly Averaged Front Lobe Efficiency (%)	3.6	2.3	0.8	1.7
Linearly Averaged Gain Penalty Relative to Free Space Gain (dB)	7.3	7.0	3.5	8.8

Table 17: RF tag antenna performance characteristics when attached to cardboard carton filled with ethylene glycol



(a) Tuned to Aluminum



(b) Tuned to Free Space

Figure 59: Three RF tag antennas attached to metal

Three RF Tag Antennas on Metal			
Tuned to Metal	<i>Baseline</i>	<i>ITO</i>	<i>Silver</i>
Linearly Averaged Front Lobe Absolute Gain (dB)	-12.8	-21.5	-18.8
Linearly Averaged Front Lobe Efficiency (%)	3.2	0.4	0.8
Linearly Averaged Gain Penalty Relative to Free Space Gain (dB)	7.8	5.9	12.0
Tuned to Free Space			
Linearly Averaged Front Lobe Absolute Gain (dB)	-12.9	-21.0	-18.8
Linearly Averaged Front Lobe Efficiency (%)	3.1	0.5	0.8
Linearly Averaged Gain Penalty Relative to Free Space Gain (dB)	8.0	5.5	12.0

Table 18: RF tag antenna performance characteristics when attached to metal

REFERENCES

- [1] K. Finkenzeller, *RFID Handbook: Fundamentals and Applications in Contactless Smart Cards and Identification*, 2nd ed. New York: John Wiley and Son LTD, 2003.
- [2] D. Kim, M. A. Ingram, and W. W. Smith Jr., “Measurements of Small-Scale Fading and Path Loss for Long Range RF Tags,” *IEEE Transactions on Antennas and Propagation*, vol. 51, no. 8, pp. 1740–1749, 2003.
- [3] K. V. S. Rao, “An Overview of Backscattered Radio Frequency Identification System (RFID),” in *1999 Asia Pacific Microwave Conference*, ser. 1999 Asia Pacific Microwave Conference. APMC’99. Microwaves Enter the 21st Century. Conference Proceedings (Cat. No.99TH8473), vol. 3. Singapore: IEEE, 1999, pp. 746–749.
- [4] I. D. Robertson and I. Jalaly, “RF ID Tagging Explained,” *Communications Engineer*, vol. 1, no. 1, pp. 20–23, 2003.
- [5] T. Purdum, “Factory to Foxhole: RFID Deadline Looms,” *Industry Week*, vol. 253, no. 11, p. 12, 2004.
- [6] S. Ricca, “Coming year critical for RFID,” *Official Board Markets*, vol. 80, no. 47, pp. 1 – 4, 2004.
- [7] Anonymous, “Wal-Mart RFID Deadline Won’t Be Met,” *Official Board Markets*, vol. 81, no. 1, p. 4, 2005.
- [8] S. Ashley, “Penny-wise Smart Labels,” *Scientific American*, vol. 291, no. 2, pp. 30–31, 2004.
- [9] M. Keskilammi, L. Sydanheimo, and M. Kivikoski, “Radio Frequency Technology for Automated Manufacturing and Logistics Control. Part 1: Passive RFID Systems and the Effects of Antenna Parameters on Operational Distance,” *International Journal of Advanced Manufacturing Technology*, vol. 21, no. 10-11, pp. 769–774, 2003.
- [10] P. F. Baude, D. A. Ender, M. A. Haase, T. W. Kelley, D. V. Muyres, and S. D. Theiss, “Pentacene-Based Radio-Frequency Identification Circuitry,” *Applied Physics Letters*, vol. 82, no. 22, pp. 3964–3966, 2003.
- [11] P. F. Baude, D. A. Ender, T. W. Kelley, M. A. Haase, D. V. Muyres, and S. D. Theiss, “Pentacene Based RFID Transponder Circuitry,” in *Device Research Conference*, ser. Device Research Conference (IEEE Cat. No.04TH8724), vol. 1. Notre Dame, IN, USA: IEEE, 2004, pp. 227–228.
- [12] W. L. Stutzman and G. A. Thiele, *Antenna Theory and Design*, 2nd ed. Hoboken, NJ: John Wiley and Sons, 1998.
- [13] T. W. Kelley, P. F. Baude, C. Gerlach, D. E. Ender, D. Muyres, M. A. Haase, D. E. Vogel, and S. D. Theiss, “Recent Progress in Organic Electronics: Materials, Devices, and Processes,” *Chemistry of Materials*, vol. 16, no. 23, pp. 4413–4422, 2004.

- [14] R. L. Li, G. DeJean, M. M. Tentzeris, and J. Laskar, "Integrable Miniaturized Folded Antennas for RFID Applications," in *IEEE Antennas and Propagation Society Symposium 2004 Digest held in Conjunction with: USNC/URSI National Radio Science Meeting*, ser. IEEE Antennas and Propagation Society, AP-S International Symposium (Digest), vol. 2. Monterey, CA, United States: Institute of Electrical and Electronics Engineers Inc., Piscataway, NJ 08855-1331, United States, 2004, pp. 1431–1434.
- [15] G. Marrocco, "Gain-Optimized Self-Resonant Meander Line Antennas for RFID Applications," *IEEE Antennas and Wireless Propagation Letters*, vol. 2, pp. 302–305, 2003.
- [16] M. Keskilammi and M. Kivikoski, "Using Text as a Meander Line for RFID Transponder Antennas," *IEEE Antennas and Wireless Propagation Letters*, vol. 3, no. 1, pp. 372–374, 2004.
- [17] U. Karthaus and M. Fischer, "Fully Integrated Passive UHF RFID Transponder IC with 16.7- μ W Minimum RF Input Power," *IEEE Journal of Solid-State Circuits*, vol. 38, no. 10, pp. 1602–1608, 2003.
- [18] J. Siden, P. Jonsson, T. Olsson, and G. Wang, "Performance Degradation of RFID System Due to the Distortion in RFID Tag Antenna," ser. 11th International Conference 'Microwave and Telecommunication Technology'. Conference Proceedings (IEEE Cat. No.01EX487). Sevastopol, Crimea, Ukraine: Weber Co, 2001, p. 3.
- [19] P. R. Foster and R. A. Burberry, "Antenna Problems in RFID Systems," in *IEE Colloquium. RFID Technology*, ser. IEE Colloquium. RFID Technology (Ref. No.1999/123). London, UK: IEE, 1999, pp. 31–35.
- [20] L. Ukkonen, L. Sydanheirno, and M. Kivikoski, "A Novel Tag Design Using Inverted-F Antenna for Radio Frequency Identification of Metallic Objects," ser. 2004 IEEE/Sarnoff Symposium on Advances in Wired and Wireless Communications (IEEE Cat. No.04EX772). Princeton, NJ, USA: IEEE, 2004, pp. 91–94.
- [21] L. Ukkonen, L. Sydanheimo, and M. Kivikoski, "Patch Antenna with EBG Ground Plane and Two-Layer Substrate for Passive RFID of Metallic Objects," in *IEEE Antennas and Propagation Society Symposium 2004 Digest held in Conjunction with: USNC/URSI National Radio Science Meeting*, ser. IEEE Antennas and Propagation Society, AP-S International Symposium (Digest), vol. 1. Monterey, CA, United States: IEEE, 2004, pp. 93–96.
- [22] B. C. Wadell, *Transmission Line Design Handbook*. Norwood, MA: Artech House, 1991.
- [23] R. W. Lampe, "Design Formulas For An Asymmetrical, Coplanar Strip, Folded Dipole," *AP-S International Symposium (Digest) (IEEE Antennas and Propagation Society)*, vol. AP-33, 1985.
- [24] R. S. Elliott, *Antenna Theory and Design*, revised ed., ser. The IEEE Press Series on Electromagnetic Wave Theory. Hoboken, NJ: John Wiley and Sons Inc., 2003.
- [25] A. Riddle, "Ferrite and wire baluns with under 1 dB loss to 2.5 GHz," in *1998 IEEE MTT-S International Microwave Symposium Digest*, vol. vol.2. Baltimore, MD: IEEE, 1998, pp. 617–620.
- [26] O. M. Woodward and S. M. Perlow, "Balance Quality Measurements on Baluns," *IEEE Transactions on Microwave Theory and Techniques*, vol. MTT-31, no. 10, pp. 821 – 824, 1983.

- [27] D. M. Pozar, *Microwave Engineering*, 3rd ed. Hoboken, NJ: John Wiley and Sons, 2005.
- [28] J. H. Sinsky and C. R. Westgate, "Design of an Electronically Tunable Microwave Impedance Transformer," in *Proceedings of the 1997 IEEE MTT-S International Microwave Symposium. Part 2 (of 3)*, ser. IEEE MTT-S International Microwave Symposium Digest, vol. 2. Denver, CO, USA: IEEE, 1997, pp. 647–650.
- [29] J. De Mingo, A. Valdovinos, A. Crespo, D. Navarro, and P. Garcia, "An RF Electronically Controlled Impedance Tuning Network Design and Its Application to an Antenna Input Impedance Automatic Matching System," *IEEE Transactions on Microwave Theory and Techniques*, vol. 52, no. 2, pp. 489–497, 2004.
- [30] A. R. V. Hippel, *Dielectric Materials and Applications*. New York: The Technology Press of M.I.T. and John Wiley and Sons, Inc., 1952.